Geometric Phases in Dissipative Quantum Systems

Aaron Daniel
Project Thesis

Dr. Martin Koppenhöfer, Prof. Dr. Christoph Bruder

Abstract

Geometric phases are of broad interest in modern physics due to their potential for robust quantum computation and their widespread occurence. In this project thesis we investigate the geometric phases arising in dissipative quantum systems exhibiting a limit cycle and their possible measurement. We show that a quantum limit-cycle system reveals a geometric phase by providing the following two new insights: First, the van der Pol spin one system, prepared in its steady state and with its quantization axis slowly rotated, attains a geometric phase that persists with finite gain and damping rates, as long as adiabaticity is retained. Secondly, through further research into the existing literature and numerical testing we found that this phase is in general not measurable in the originally envisaged way through a Mach-Zehnder interferometer.

Department of Physics
University of Basel
Switzerland

Contents

Introduction

Geometry has always had a central place in both mathematics and physics. It helps us understand deep connections in our universe by engaging the large visual part of our brain, it again and again puts natures laws in exceptionally elegant form and it often stands outside of time by considering the inherent properties of shapes and spaces. In quantum systems geometry manifests itself through the structure of the Hilbert space which is the state space of physical systems in quantum mechanics. In this project thesis we treat geometric phases which arise as a consequence of the evolution of quantum states through this space. These phases embody the aforementioned characteristics of geometry beautifully and may in the future serve as a way of achieving robust quantum computation [13]. We treat geometric phases arising in the evolution of quantum systems that are in contact with an environment. These phases owe their name to the fact that they are not a product of time evolution but are a geometric property of the state space of the system under consideration. More precisely we will consider geometric phases of a quantum system exhibiting a limit cycle in phase space, namely the van der Pol spin one system introduced in [12]. In this endeavour we build on the work done in the masters thesis *Geometric Phases in Limit-Cycle Systems* by Lea Fricker under the supervision of Prof. Christoph Bruder and Dr. Alexandre Roulet [6]. Building on their work concerning the limiting case of a system without coupling to the environment we focus on extending the calculation of geometric phases to the case of systems interacting with the environment. We also investigate the possibility of experimentally detecting these geometric phases in an interferometer and discuss the approach to predict the outcome of such an experiment.

Chapter 1

Theoretical Background

Though seldomly treated in undergraduate courses, geometric phases (GP) are a recurring phenomenon in both classical and quantum physics. They appear in simple mechanical systems, see Subsection 1.1, in condensed matter systems, in quantum-chemistry, cold atoms and more [14]. They are phases picked up by a system that undergoes cylic adiabatic evolution and are generally due to the geometry of the underlying parameter space. Since Berry [2] showed in 1984 that for the case of cyclic adiabatic evolution of non-degenerate quantum states, the quantum geometric phase too is a consequence of parameter space geometry, it has received much attention. Our focus here lies on the case of geometric phases arising in dissipative quantum systems. Quantum states in such systems are in general mixed states and a generalization of the geometric phase for pure states to mixed states is needed. In this chapter we first provide some intuition using an example from classical physics, then explain the concept of geometric phases for pure states and detail two notions of geometric phases for mixed states. An extensive introduction to the topic of geometric phases in physics can be found in [3], [1] or [4].

1.1 Classical Example

To gain some intuition on the geometric phase we will work through a classical example of a geometric phase, mentioned in [1], namely the Foucault pendulum. We will follow the general treatment of the problem in [18] here but shorten the derivation of the geometric phase using basic notions of differential geometry. The Foucault pendulum is a simple pendulum suspended high above the ground and set into planar motion. We will in the following model earth as the 2-sphere S^2 embedded in $\mathbb{R}^3$ and equipped with a notion of parallel transport through the Levi-Civita connection. Further we neglect non-isotropic friction and we assume that the motion of the pendulum is restricted to the plane of oscillation which passes through the center of the sphere. This assumption is sometimes called the assumption of adiabaticity because it is justified if the frequency of the pendulums oscillation is much larger than the frequency of earths rotation [18]. The metric on the sphere expressed through standard spherical coordinates is as follows,

$$g = r^2 d\theta^2 + r^2 \sin^2\theta^2 d\phi^2. \tag{1.1}$$

With the Levi-Civita connection we obtain the Christoffel symbols,

$$\Gamma^{\phi}_{\phi\theta} = \Gamma^{\phi}_{\theta\phi} = \frac{\cos\theta}{\sin\theta}, \tag{1.2}$$

$$\Gamma^{\theta}_{\phi\phi} = -\sin\theta\cos\theta, \tag{1.3}$$

the other Γ^{i}_{jk} vanish. We now model the orientation of the plane of oscillation by a vector p at fixed angle θ_0 that is being parallely transported around the sphere, i.e. along the ϕ coordinate. In order to be parallely transported along the ϕ coordinate, p must satisfy the parallel transport condition,

$$\left(\nabla_{\frac{\partial}{\partial\phi}} p\right)^{\alpha} = \frac{\partial}{\partial\phi} p^{\alpha} + \Gamma^{\alpha}_{\beta\gamma} p^{\beta}. \tag{1.4}$$

With the Christoffel symbols from above this leads to two differential equations,

$$\frac{\partial}{\partial\phi} p^{\theta} - \sin\theta\cos\theta\, p^{\phi} = 0, \tag{1.5}$$

$$\frac{\partial}{\partial\phi} p^{\phi} + \frac{\cos\theta}{\sin\theta} p^{\theta} = 0, \tag{1.6}$$

which can be solved to find the general solution,

$$p^{\theta} = a\cos(\phi\cos\theta) + b\sin(\phi\cos\theta), \tag{1.7}$$

$$p^{\phi} = -a\frac{\sin(\phi\cos\theta)}{\sin\theta} + b\frac{\cos(\phi\cos\theta)}{\sin\theta} \quad a, b \in \mathbb{R}. \tag{1.8}$$

From now on we use the canonical basis $\{\partial_\theta, \partial_\phi\}$ of the tangent space defined at each point. Inserting the condition that the pendulum initially oscillates from north to south, i.e. $p = \partial_\theta|_{(\theta_0,0)}$, and starts at $\theta = \theta_0$ we get the solution,

$$p^{\theta} = \cos(\phi\cos\theta_0), \quad p^{\phi} = -\frac{\sin(\phi\cos\theta_0)}{\sin\theta_0}. \tag{1.9}$$

After being parallely transported once around the sphere, i.e. $\phi = 2\pi$, p has the following form,

$$p = \cos(2\pi\cos(\theta_0))\ \partial_\theta|_{(\theta_0,2\pi)} - \frac{\sin(2\pi\cos\theta_0)}{\sin\theta_0}\ \partial_\phi|_{(\theta_0,2\pi)}\,, \tag{1.10}$$

which is in general not equal to the initial p. We can further compute the angle γ between p before and after the revolution to find the angle by which the plane of oscillation differs after one rotation of the earth around its axis:

$$\gamma = \cos^{-1}\left(\frac{p_0 \cdot p_{2\pi}}{|p_0||p_{2\pi}|}\right) = 2\pi\cos\theta_0. \tag{1.11}$$

Equivalently this result can be expressed as $\gamma = -2\pi\sin(\lambda)$ with λ being latitude. With that we recover the result from [18]. This result and the approach we took to arive at it highlight the fact that the geometric phase, here the rotation angle of the plane of oscillation, is a consequence of geometry and independent of time. From our derivation it is evident that the time it takes the earth to rotate is irrelevant to the phase γ, as long as the assumption of adiabaticity

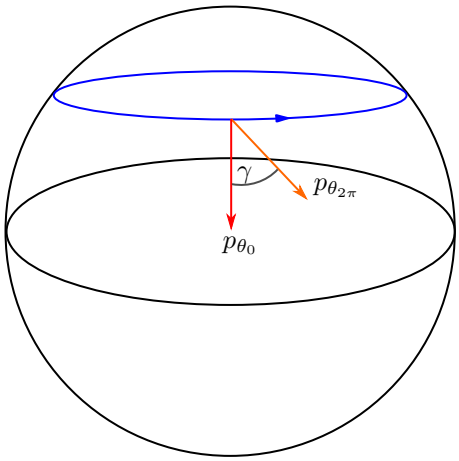

Figure 1.1: Sketch of the geometric phase γ aquired when the vector p_{θ_0} is parallely transported along ϕ by 2π.

holds. In this particular case, the geometric phase arises due to the curvature of the sphere. Being transported in ordinary two-dimensional Euclidean space, the plane of rotation of the Foucault pendulum would have been fixed. Moreover considering our result one finds that the geometric phase γ vanishes at the poles and at the equator, hinting at a possible connection to the solid angle enclosed by the path. This connection can be made explicit using the Gaus-Bonnet theorem and finds application in the treatment of geometric phases for generic two-level Hamiltonians such as a Quantum Bit (Qubit) [2].

1.2 Pure State Geometric Phase

1.2.1 Berry Phase

Before diving into the more complicated case of mixed states we will partly reproduce the seminal result by Berry on geometric phases of pure states [2]. In his paper published in 1984 he derived an explicit formula to compute the geometric phase of a non-degenerate quantum system undergoing cyclic adiabatic unitary evolution. Even more importantly he showed that this phase only depends on the geometry of the parameter space and is gauge-invariant.
Let us consider a Hamiltonian $\hat{H}$ that depends on a set of parameters $\vec{R} = (R_1, \ldots, R_k) \in \mathbb{R}^k$ and suppose that we know the eigenvalues and eigenstates of this Hamiltonian depending on the parameters,

$$\hat{H}(\vec{R}) \left| n(\vec{R}) \right\rangle = E_n(\vec{R}) \left| n(\vec{R}) \right\rangle . \tag{1.12}$$

The parameters $\vec{R}$ can themselves depend on time and evolution of the system between $t = 0$ and $t = T$ corresponds to a path $\Gamma : [0, T] \to \mathbb{R}^k$, $t \mapsto \vec{R}(t)$ in the space of parameters. A state of this system $|\psi(t)\rangle$ prepared in one of the

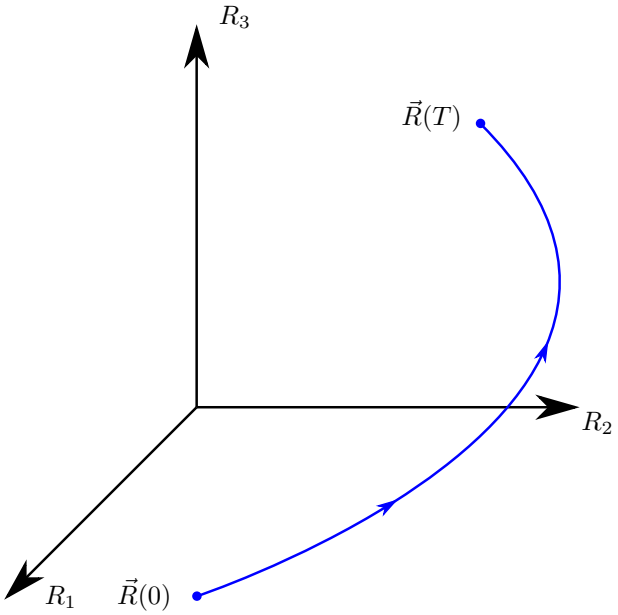

Figure 1.2: The path Γ in blue, traversed in parameter space during the evolution of the system in time from $t = 0$ to $t = T$.

eigenstates $\left|n(\vec{R}(0))\right\rangle$ obeys the Schrödinger equation,

$$\hat{H}(\vec{R}(t))\,|\psi(t)\rangle = i\hbar\frac{\partial}{\partial t}\,|\psi(t)\rangle\,, \tag{1.13}$$

and if evolved adiabatically will remain an instantaneous eigenstates of the Hamiltonian and be in the state $\left|n(\vec{R}(t))\right\rangle$ at time t. We can therefore write $|\psi(t)\rangle$ as follows,

$$|\psi(t)\rangle = e^{-\frac{i}{\hbar}\int_0^t E_n(\vec{R}(s))ds} e^{i\gamma_n(t)}\left|n(\vec{R}(t))\right\rangle. \tag{1.14}$$

The first exponential contains the well-known *dynamical phase* while the second exponential contains the *geometric phase* $\gamma_n(t)$. Inserting Eq. (1.14) into Eq. (1.13) we get the following condition on $\gamma_n(t)$:

$$\dot{\gamma}_n(t) = i\left\langle n(\vec{R}(t))\right|\frac{\mathrm{d}}{\mathrm{d}t}\left|n(\vec{R}(t))\right\rangle = i\left\langle n(\vec{R}(t))\middle|\nabla_{\vec{R}} n(\vec{R}(t))\right\rangle\cdot\dot{\vec{R}}(t). \tag{1.15}$$

Integrating this expression and substituting $\vec{R}(t)$ in the integral we find that the geometric phase γ_n loses its dependence on time,

$$\gamma_n(\Gamma) = i\int_\Gamma \left\langle n(\vec{R})\middle|\nabla_{\vec{R}} n(\vec{R})\right\rangle\cdot d\vec{R}. \tag{1.16}$$

So we see that this phase factor is indeed only depending on the path Γ in parameter space and completely independent on how that path is traversed in time. Now in order to be a measurable quantity this phase has to be gauge-invariant – at least under certain conditions to be specified. For that we consider a second state $|\psi'(t)\rangle$ also prepared in an eigenstate but different from our previous state by a complex number of modulus one,

$$|\psi'(t)\rangle = e^{-i\theta(\vec{R})}\,|\psi(t)\rangle\,, \tag{1.17}$$

where $\theta(\vec{R})$ is an arbitrary function. By the same procedure as above we find that the geometric phase γ'_n belonging to this state has to fulfill the condition,

$$\begin{aligned}\dot{\gamma'}_n(t) &= i \langle n(R(t))| e^{-i\theta(\vec{R})} \left|\nabla_{\vec{R}} e^{-i\theta(t)} n(\vec{R}(t))\right\rangle \dot{\vec{R}}(t) \\ &= i\Big(\Big\langle n(\vec{R}(t))\Big|\nabla_{\vec{R}} n(\vec{R}(t))\Big\rangle + \nabla_{\vec{R}}\theta(\vec{R})\Big)\dot{R}(t). \end{aligned} \tag{1.18}$$

Integrating this we find,

$$\gamma'_n(\Gamma) = \gamma_n(\Gamma) + \theta(\vec{R}(0)) - \theta(\vec{R}(T)), \tag{1.19}$$

and hence the geometric phase γ_n is in general not gauge-invariant. For a closed path C however we have $\vec{R}(0) = \vec{R}(T)$ which leads to $\gamma'_n = \gamma_n$ so in this particular case the geometric phase is gauge-invariant. In a three-dimensional parameter space this result can be derived even more elegantly using basic vector calculus. In the case of a closed loop, Eq. (1.16) shows an integral along a closed curve C that bounds a surface S. This integral can be rewritten into a surface integral using Stokes theorem,

$$\gamma_n(C) = i \oint_C \Big\langle n(\vec{R})\Big|\nabla_{\vec{R}} n(\vec{R})\Big\rangle d\vec{R} = i \oiint_S \Big(\vec{\nabla} \times \Big\langle n(\vec{R})\Big|\nabla_{\vec{R}} n(\vec{R})\Big\rangle\Big) d\vec{a}. \tag{1.20}$$

If we now look at how the integrand changed under gauge transformations, we find that the only term we had to add was the gradient of a function which vanishes in the surface integral. Due to this, the term $i\left\langle n(\vec{R})\middle|\nabla_{\vec{R}} n(\vec{R})\right\rangle$ is sometimes called the Berry vector potential.

1.2.2 Pancharatnam Phase

In preparation of the more general case of geometric phases for mixed states we need to mention the Pancharatnam relative phase and how the Berry phase relates to it. We showed above that the Berry phase is only gauge-invariant if the evolution of the underlying system is cyclic and therefore a reasonable notion of geometric phase was only possible for this scenario. After Berrys discovery, the concept of geometric phases was extended to arbitrary pure state evolution by building on the work of S. Pancharatnam on geometric phases of polarized beams passing through cystals. To explain that connection we shorten and repeat the respective section in [14]. Let $|\phi(0)\rangle$ and $|\phi(\tau)\rangle$ be two non-orthogonal states on a path $\Gamma\colon [0,\tau] \to \mathcal{H},\ t \mapsto |\phi(t)\rangle$. The relative phase between these two states is given by the Pancharatnam relative phase $\arg(\langle\phi(0)|\phi(\tau)\rangle)$ and can be seen as the global phase that contains both the dynamic and geometric contributions aquired during the evolution along Γ. With the same idea we can define local phase changes as the following limit,

$$\lim_{\delta t \to 0} \int_0^\tau \arg(\langle\phi(t)|\phi(t+\delta t)\rangle) dt = -i \int_0^\tau \Big\langle \phi(t)\Big|\dot{\phi}(t)\Big\rangle\, dt. \tag{1.21}$$

If we now subtract the local phase changes from the global phase change we end up with the geometric phase,

$$\gamma[\Gamma] = \arg(\langle\phi(0)|\phi(\tau)\rangle) + i \int_0^\tau \Big\langle \phi(t)\Big|\dot{\phi}(t)\Big\rangle\, dt. \tag{1.22}$$

This geometric phase is invariant under gauge transformations [15] and applies to any path Γ with nonorthogonal endpoints $|\psi(0)\rangle, |\psi(\tau)\rangle$. The Berry phase, seen from this perspective, corresponds to the following special phase choice,

$$|\psi(t)\rangle = e^{-i\arg(\langle\phi(0)|\phi(t)\rangle)}\,|\phi(t)\rangle\,. \tag{1.23}$$

For cyclic evolution we have $\arg(\langle\psi(0)|\psi(\tau)\rangle) = 0$ and hence the geometric phase is,

$$\gamma[\Gamma] = i\int_0^\tau \left\langle \psi(t)\middle|\dot{\psi}(t)\right\rangle dt, \tag{1.24}$$

as found in Eq. (1.16).

1.2.3 Parallel Transport

In the framework of global and local phase changes presented above, we can define a notion of parallel transport for pure states. This is analogous to the condition we set by demanding that our vector fulfills the parallel transport condition in the classical example of the Foucault pendulum. Parallel transport of a pure state simply refeers to the state not picking up any phase between t and $t+\delta t$ along its way. These are exactly the local phase changes and hence, parallel transport means that no local phases are being picked up or equivalently,

$$\left\langle \phi(t)\middle|\dot{\phi}(t)\right\rangle = 0, \quad t\in[0,\tau) \Rightarrow i\int_0^\tau \left\langle \phi(t)\middle|\dot{\phi}(t)\right\rangle dt = 0. \tag{1.25}$$

If this condition is fulfilled, $|\phi(t)\rangle$ is said to be parallely transported and the geometric phase equals the Pancharatnam relative phase. Therefore if one wants to measure a geometric phase in an interferometer, see Fig. 1.3, one has to ensure either that the system is parallely transported or that the dynamical phase is a multiple of 2π. In both cases only the geometric phase remains as the relative phase accumulated during the evolution.

1.3 Geometric Phases for Mixed States

We now turn to the more general concept of geometric phases for mixed states. For this extension the two notions of Pancharatnam phase and parallel transport from the pure state geometric phase will prove to be crucial, since the extension follows this general procedure:

1. Define a concept of relative phase between mixed states,
2. set parallel transport conditions to fix the independent phase factors,
3. measure the geometric phase when these conditions are met, i.e. when the relative phase equals the geometric phase.

1.3.1 Geometric Phases for Mixed States in Interferometry

To measure the geometric phase of a system one has to perform interference measurements. This way the system that has undergone a time evolution aquiring some geometric phase can be compared to the same system before and the

geometric phase will become visible in the interference pattern. A reasonable idea to extend the notion of geometric phases to mixed states is thus to orient oneself on this relation to interference experiments. This approach was taken in [15] to introduce the total phase of a mixed state undergoing unitary evolution. It turns out that one can find this geometric phase as the coherent average over the pure states for an initially diagonal mixed state. We will eventually be interested in the geometric phase of a mixed state undergoing non-unitary evolution but will first consider the unitary case here. We start by considering a conventional Mach-Zehnder interferometer (MZI) as seen in Fig. 1.3. We model the beam entering this interferometer by a two dimensional Hilbert space $\mathcal{H}_B = \{|0\rangle, |1\rangle\}$ and represent the beam splitters, mirrors and relative phase shifts by unitary operators in its basis.

$$\begin{aligned}
\hat{U}_{M_B} &= |1\rangle\langle 0| + |0\rangle\langle 1|, \\
\hat{U}_{BS_B} &= \frac{1}{\sqrt{2}}(|0\rangle\langle 0| + |0\rangle\langle 1| + |1\rangle\langle 0| - |1\rangle\langle 1|), \\
\hat{U}_{PS_B} &= e^{i\chi}|0\rangle\langle 0| + |1\rangle\langle 1|.
\end{aligned} \tag{1.26}$$

For a state $\hat{\rho}_{B_{in}} = |0\rangle\langle 0|$ going into the MZI, the output state,

$$\hat{\rho}_{B_{out}} = \frac{1}{2}((1+\cos\chi)|0\rangle\langle 0| + \sin\chi|0\rangle\langle 1| - \sin\chi|1\rangle\langle 0| + (1-\cos\chi)|1\rangle\langle 1|),$$

gives rise to a firing probability $p_0 = \frac{1}{2}(1+\cos\chi)$. The relative phase shift χ can therefore be detected in the firing probabilities p_0, p_1. Our goal now is to derive an expression for the firing probabilities if additional degrees of freedom of a system entering the MZI experience a unitary time evolution in the upper arm. To do this we consider a second Hilbert space of the system S, $\{|k\rangle_S\}_k$. We further assume that the initial density operator of the system is diagonal in this basis,

$$\hat{\rho}_{0_S} = \sum_{k=1}^{N} \omega_k |k\rangle\langle k|, \tag{1.27}$$

and can change inside the interferometer, being acted on by a unitary operator,

$$\hat{\rho}_{0_S} \to \hat{U}_S \hat{\rho}_{0_S} \hat{U}_S^\dagger. \tag{1.28}$$

The operators describing the beam splitters, mirrors and the phase shift leave the state of the internal system unchanged and can be lifted into the combined Hilbert space, $\hat{U}_M = \hat{U}_{M_B} \otimes \hat{I}_S$, $\hat{U}_{BS} = \hat{U}_{BS_B} \otimes \hat{I}_S$. We further introduce the unitary operator,

$$\hat{U} = |1\rangle\langle 1| \otimes \hat{U}_S + e^{i\chi}|0\rangle\langle 0| \otimes \hat{I}_S, \tag{1.29}$$

to describe the time evolution inside the interferometer. For a state

$$\hat{\rho}_{in} = |0\rangle\langle 0| \otimes \hat{\rho}_{S_{in}} \tag{1.30}$$

going into the interferometer, we now get the outgoing state,

$$\hat{\rho}_{out} = \hat{U}_B \hat{U}_M \hat{U} \hat{U}_B \hat{\rho}_{in} \hat{U}_B^\dagger \hat{U}^\dagger \hat{U}_M^\dagger \hat{U}_B^\dagger, \tag{1.31}$$

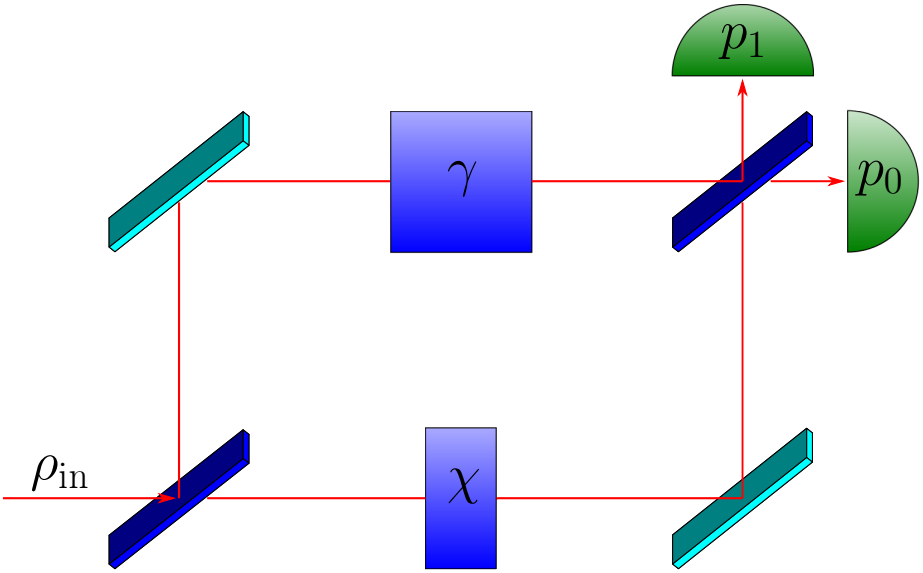

Figure 1.3: Setup of a MZI. It consists of two beam splitters (dark blue) and two mirrors (cyan). The combined state of the beam and the internal system enters the MZI, the beam experiences a phase shift χ in the lower arm whereas the internal system undergoes an evolution aquiring a phase γ in the upper arm. The two detectors (green) measure wether the state exits the second beam splitter in the horizontal or vertical direction.

which yields the firing probability p_0 as follows,

$$p_0 = \frac{1}{2}\Big[1 + |\mathrm{Tr}(\hat{U}_S\hat{\rho}_{S_{in}})|\cos\Big(\chi - \arg\Big(\mathrm{Tr}(\hat{U}_S\hat{\rho}_{S_{in}})\Big)\Big)\Big]. \tag{1.32}$$

The interference oscillations produced by the phase shift χ are thus shifted by $\phi = \arg\Big(\mathrm{Tr}(\hat{U}_S\hat{\rho}_{S_{in}})\Big)$ and this phase difference reduces to the Pancharatnam phase difference for pure states [15]. The additional phase shift ϕ can be considered the relative phase of the mixed state $\hat{\rho}_S$ aquired during the evolution represented by $\hat{U}_S$. We leave out the exact treatment on the parallel transport conditions, this can be found in [15]. In short we demand that each eigenstate of the mixed state is itself parallely transported, meaning it obeys the condition in Eq. (1.25) . When these parallel transport conditions are met, the relative phase ϕ equals the geometric phase of the mixed state $\hat{\rho}_S$ and can be detected in the interferometer.

1.3.2 Kinematic Approach to the Mixed State Geometric Phase in Nonunitary Evolution

We now turn to the notion of geometric phases for mixed states undergoing non-unitary, hence dissipative, evolution. The central idea will be the one of *purification*. The mixed state is represented by a pure state in a higher dimensional Hilbert space whose partial trace over the ancillary Hilbert space reproduces the original mixed state. One then considers the Pancharatnam relative

phase of this purified state under additional parallel transport conditions. This process makes use of an ancilla that is not unique and in general the geometric phase of a mixed state in nonunitary evolution will depend on this ancilla [11], [5]. A straightforward generalization of the interference measurement presented above where only the system itself and not the ancilla is considered, is therefore not possible. In this subsection we will reproduce the approach to the geometric phase for mixed states in nonunitary evolution that was proposed in [17]. Most importantly we derive a formula for the geometric phase of a mixed state undergoing nonunitary, nondegenerate evolution. We consider a quantum system with N-dimensional Hilbert space. An evolution of the state of the system may be described as the path,

$$\mathcal{P}\colon t \in [0,\tau] \to \hat{\rho}(t) = \sum_{k=1}^{N} \omega_k(t)\, |\phi_k(t)\rangle \langle\phi_k(t)|\,, \tag{1.33}$$

where the eigenvalues $\omega_k(t)$ are assumed to be non-negative and non-degenerate. The case of degenerate eigenvalues is treated in [17] but will not concern us in this report. The first step in deriving a formula for the geometric phase γ, associated to the path $\mathcal{P}$ in the Hilbert space $\mathcal{H}$ of the quantum system, is to lift the state to a pure state in a larger Hilbert space. This procedure called *purification* means we consider the combined Hilbert space $\mathcal{H} \otimes \mathcal{H}_a$ of our systems and an ancillary system a. The purification is chosen such that the original state $\hat{\rho}(t)$ can at all times be obtained from the purified state $|\Psi(t)\rangle$ by taking the partial trace of $|\Psi(t)\rangle \langle\Psi(t)|$ over the ancilla a. We will assume in the following that the dimension of the ancillas Hilbert space equals that of the systems Hilbert space. The purified state is then given by,

$$|\Psi(t)\rangle = \sum_{k=1}^{N} \sqrt{\omega_k(t)}\, |\phi_k(t)\rangle \otimes |a_k\rangle \in \mathcal{H} \otimes \mathcal{H}_a, \quad t \in [0,\tau]. \tag{1.34}$$

To assign a geometric phase to the mixed state $\rho(t)$ we now consider the Pancharatnam relative phase between the purified state at time zero $|\Psi(t)\rangle$ and the purified state at time τ, $|\Psi(\tau)\rangle$,

$$\alpha(t) = \arg(\langle\Psi(0)|\Psi(\tau)\rangle) = \arg\left(\sum_{k=1}^{N} \sqrt{\omega_k(0)\omega_k(\tau)}\, \langle\phi_k(0)|\phi_k(\tau)\rangle\right). \tag{1.35}$$

Using the orthonormality of the bases $\{|\phi_k(0)\rangle\}$, $\{|\phi_k(\tau)\rangle\}$ we rewrite this phase as follows,

$$\alpha(t) = \arg(\langle\Psi(0)|\Psi(\tau)\rangle) = \arg\left(\sum_{k=1}^{N} \sqrt{\omega_k(0)\omega_k(\tau)}\, \langle\phi_k(0)|\, \hat{V}(\tau)\, |\phi_k(0)\rangle\right), \tag{1.36}$$

with

$$\hat{V}(t) = |\phi_1(t)\rangle \langle\phi_1(0)| + \cdots + |\phi_N(t)\rangle \langle\phi_N(0)|\,. \tag{1.37}$$

With the geometric phase being an inherent property of the path $\mathcal{P}$ only we need to remove the dependency of the phase $\alpha(t)$ on the purification. We do this by noting that there is an equivalence set $\mathcal{S}$ of unitaries $\hat{\tilde{V}}(t)$ that realize

the path $\mathcal{P}$,

$$\tilde{\hat{V}}(t) = \hat{V}(t) \sum_{k=1}^{N} e^{i\theta_k(t)} \left|\phi_k(0)\right\rangle \left\langle\phi_k(0)\right|, \tag{1.38}$$

where $\theta_k(t)$ are real time-dependent parameters that fulfill $\theta_k(0) = 0$. We now choose $\hat{V}^{\parallel}(t) \in S$ such that the parallel transport conditions

$$\left\langle\phi_k(0)\right| \hat{V}^{\parallel\dagger}(t)\dot{\hat{V}}^{\parallel}(t) \left|\phi_k(0)\right\rangle = 0, \quad k = 1, \ldots, N, \tag{1.39}$$

are fulfilled. In the case where these parallel transport conditions are fulfilled, the relative phase $\alpha(t)$ equals the geometric phase $\gamma[\mathcal{P}]$. This choice determines the time-dependent parameters,

$$\theta_k(t) = i \int_0^t \left\langle\phi_k(0)\right| \hat{V}^{\dagger}(s)\dot{\hat{V}}(s) \left|\phi_k(0)\right\rangle \, ds. \tag{1.40}$$

Taking this expression for $\hat{V}(t)$ we obtain the formula for the geometric phase γ associated to the path $\mathcal{P}$,

$$\gamma[\mathcal{P}] = \arg\left(\sum_{k=1}^{N} \sqrt{\omega_k(0)\omega_k(\tau)} \left\langle\phi_k(0)|\phi_k(\tau)\right\rangle e^{-\int_0^\tau \left\langle\phi_k(t)|\dot{\phi}_k(t)\right\rangle dt} \right). \tag{1.41}$$

This notion of the geometric phase fulfills the following conditions: It is gauge invariant, it reduces to known results for unitary evolution and it is experimentally testable in principle [17]. Interpreting this formula in the context of pure state geometric phases one could say that the geometric phase here is the sum over the geometric phases of each eigenstate. From the global phase of each eigenstate $\langle\phi_k(0)|\phi_k(\tau)\rangle$ we subtract the local phase changes $-i\int_0^\tau \left\langle \phi_k(t)\middle|\dot{\phi}_k(t)\right\rangle dt$ by multiplication with the exponential. In the case where our system is parallely transported, we have $\alpha(\tau) = \gamma[\Gamma]$ and the geometric phase can be measured in an interferometer where the purified state $\Psi(0)$ is used as an input state. Further details on the evolution $\Psi(0)$ undergoes can be found in [17].

1.4 Limit Cycle

We recall this concept here because the van der Pol spin one system treated in Section 3.3 is a system exhibiting a limit cycle. Limit cycles are closed trajectories in the phase space of a dynamical system that attract at least one other trajectory [16]. They appear in the study of nonlinear systems and often come as attractors of differential equations modelling self-sustained oscillation. Self-sustained oscillators are an example of classical dissipative systems where an internal supply of energy keeps the oscillations of a dissipative system going. Trajectories on the limit cycle are stable with regards to their amplitude and neutral with regards to their phase. Systems exhibiting limit cycles therefore lend themselves to synchronization. The concept of the limit cycle in the quantum case is analogous to the classical case as has been demonstrated in [7].

Chapter 2

Theoretical Analysis

2.1 Semi-analytical Formula

Solutions to dissipative quantum systems in closed analytical form are rare and beyond the simplest models it is often impossible to solve the differential equations arising from the Quantum Master Equation (QME) by hand. To nonetheless be able to compute the geometric phase for mixed states in non-unitary evolution, we opted for a semi-analytical approach. We employ a numerical solver provided by the *QuantumOptics.jl* package in *Julia* to get the time evolution of our system. For an elementary example of this procedure, see Appendix C. We then diagonalize the density matrix for each timestep and using numerical differentiation and integration compute the terms of Eq. (1.41). When diagonalizing we adopt the convention that the first entry of each eigenstate is real. This means we always use the convention for the Berry phase because the eigenstates cannot pick up a local phase and the Pancharatnam phase will vanish for a closed path. The differentiation is done using a fourth-order symmetrical

Algorithm 1: Semi-analytical calculation of the geometric phase (GP)

Input : H, ρ_0, parameters
Output: GP

1 Compute time evolution $\rho_t = [\rho(t_1), \rho(t_2), \ldots, \rho(t_n)]$;
2 Compute the eigenstates $|\phi_k(t_i)\rangle$ and eigenvalues $\omega_k(t_i)$ for each $\rho(t_i)$;
3 Differentiate the eigenstates to obtain $\left|\dot{\phi}_k(t_i)\right\rangle$;
4 Integrate $\left\langle \phi_k \middle| \dot{\phi}_k \right\rangle$ over time;
5 Compute GP using Eq. (1.41).

difference quotient and the integration is done using the extended Simpson rule. For details on the implementation of the numerical procedures see Appendix C. We will test this approach to computing the geometrical phase in the case of pure Qubit dephasing, Sec. 3.2, and the van der Pol spin one system, Sec. 3.3.

2.2 Rotating Frame

The second system we consider in this chapter is the van der Pol limit cycle oscillator whose quantization axis is slowly rotated. This means that the Hamiltonian $\hat{H}(t)$ and the jump operators $\hat{\Gamma}_i(t)$ are rotated, i.e. $\hat{H}(t) = \hat{R}(t)\hat{H}_0\hat{R}^\dagger(t)$, $\hat{\Gamma}_i(t) = \hat{R}(t)\hat{\Gamma}_{0_i}\hat{R}^\dagger(t)$ (see Fig. 3.2). We now derive approximate formulas for the geometric phase in this scenario using perturbation theory. We consider a time-dependent rotation operator $\hat{R}(t)$ that acts as a transformation to a rotating frame and is unitary. The initial QME is given as follows,

$$i\hbar\frac{\mathrm{d}}{\mathrm{d}t}\hat{\rho}(t) = \Big[\hat{H}(t), \hat{\rho}(t)\Big] + \sum_i \mathcal{D}\Big[\hat{\Gamma}_i(t)\Big]\hat{\rho}(t), \tag{2.1}$$

$$\mathcal{D}\Big[\hat{\Gamma}\Big]\hat{\rho} = \hat{\Gamma}\hat{\rho}\hat{\Gamma}^\dagger - \frac{1}{2}\Big\{\hat{\Gamma}^\dagger\hat{\Gamma}, \hat{\rho}\Big\},$$

and the mixed state is assumed to transform as,

$$\hat{\rho}(t) = \hat{R}(t)\hat{\rho}_{\mathrm{rot}}(t)\hat{R}^\dagger(t). \tag{2.2}$$

Then the transformed density matrix $\hat{\rho}_{\mathrm{rot}}(t)$ obeys the following equation,

$$i\hbar\frac{\mathrm{d}}{\mathrm{d}t}\hat{\rho}_{\mathrm{rot}}(t) = \Big[\hat{R}(t)^\dagger\hat{H}(t)\hat{R}(t) - i\hbar\hat{R}^\dagger(t)\frac{\partial}{\partial t}\hat{R}(t), \hat{\rho}_{\mathrm{rot}}(t)\Big] \tag{2.3}$$

$$+ \sum_i \mathcal{D}\Big[\hat{R}^\dagger(t)\hat{\Gamma}_i(t)\hat{R}(t)\Big]\hat{\rho}_{\mathrm{rot}}(t). \tag{2.4}$$

For our Hamiltonian and Lindblad operators as assumed above, Eq. (2.4) takes the following form,

$$i\hbar\frac{\mathrm{d}}{\mathrm{d}t}\hat{\rho}_{\mathrm{rot}}(t) = \Big[\hat{H}_0 - i\hbar\hat{R}^\dagger(t)\frac{\partial}{\partial t}\hat{R}(t), \hat{\rho}_{\mathrm{rot}}(t)\Big] + \sum_i \mathcal{D}\Big[\hat{\Gamma}_{0_i}\Big]\hat{\rho}_{\mathrm{rot}}(t). \tag{2.5}$$

To obtain solutions for $\hat{\rho}(t)$ one can now solve for $\hat{\rho}_{\mathrm{rot}}(t)$ and then use Eq. (2.2) to get $\hat{\rho}(t)$.

2.2.1 Perturbative Solutions

Additional to the rotating frame approach we employed perturbation theory to obtain solutions to for the steady state in the van der Pol spin one system. For notational purposes we will denote the density matrix in the rotated frame as $\hat{\chi}(t)$ from now on. We expanded $\hat{\chi}(t)$ into a power series in ω,

$$\hat{\chi}(t) = \hat{\chi}^{(0)}(t) + \omega\hat{\chi}^{(1)}(t) + \ldots, \tag{2.6}$$

and focused only on linear terms in ω to get an approximation for slow rotations,

$$\hat{\chi}(t) \approx \hat{\chi}^{(0)}(t) + \omega\hat{\chi}^{(1)}(t). \tag{2.7}$$

For a Hamiltonian consisting of an unperturbed part $\hat{H}_0$ and a linear perturbation in ω,

$$\hat{H} = \hat{H}_0 - i\hbar\hat{R}^\dagger(t)\frac{\partial}{\partial t}\hat{R}(t) := \hat{H}_0 + \omega\hat{H}_1, \tag{2.8}$$

this leads to two differential equations for $\hat{\chi}^{(0)}$ and $\hat{\chi}^{(1)}(t)$,

$$\begin{aligned}\frac{\mathrm{d}}{\mathrm{d}t}\hat{\chi}^{(0)}(t) &= -\frac{i}{\hbar}\Big[\hat{H}_0, \hat{\chi}^{(0)}(t)\Big] + \sum_i \mathcal{D}\Big[\hat{\Gamma}_{0_i}\Big]\hat{\chi}^{(0)}(t), \\ \frac{\mathrm{d}}{\mathrm{d}t}\hat{\chi}^{(1)}(t) &= -\frac{i}{\hbar}\Big[\hat{H}_0, \hat{\chi}^{(1)}(t)\Big] - \frac{i}{\hbar}\Big[\hat{H}_1, \hat{\chi}^{(0)}(t)\Big] + \sum_i \mathcal{D}\Big[\hat{\Gamma}_{0_i}\Big]\hat{\chi}^{(1)}(t), \end{aligned} \tag{2.9}$$

where the first one is just the QME for the unperturbed Hamiltonian $\hat{H}_0$. Expanding $\hat{\chi}^{(0)}$ and $\hat{\chi}^{(1)}$ in the basis of Gell-Mann matrices $\hat{\lambda}_i$,

$$\hat{\chi}^{(0)}(t) = \frac{1}{3}\left(\mathbb{1} + \sum_{i=1}^{8} c_i(t)\hat{\lambda}_i\right), \quad \hat{\chi}^{(1)}(t) = \frac{1}{3}\left(b_0(t)\mathbb{1} + \sum_{i=1}^{8} b_i(t)\hat{\lambda}_i\right), \tag{2.10}$$

one can derive differential equations for the coefficients $\{c_i\}, \{b_i\}$. In the case of the van der Pol system it suffices to derive the steady state $\hat{\chi}_{\text{steady}}$ since the rotation is performed adiabatically. Having determined both coefficients $\hat{\chi}^{(0)}_{\text{steady}}$, $\hat{\chi}^{(1)}_{\text{steady}}$ of the steady state we use that $\hat{\chi}^{(0)}_{\text{steady}}$ is diagonal and employ time-independent nondegenerate perturbation theory to obtain the eigenvalues and eigenvectors of $\hat{\chi}_{\text{steady}}$ to first order in ω,

$$w_k \approx w_k^{(0)} + \omega \left\langle v_k^{(0)} \right| H_1 \left| v_k^{(0)} \right\rangle, \tag{2.11}$$

$$|v_k\rangle \approx \left|v_k^{(0)}\right\rangle + \omega \sum_{j\neq k} \left|v_j^{(0)}\right\rangle \frac{\left\langle v_j^{(0)}\right| H_1 \left|v_k^0\right\rangle}{w_k^0 - w_j^0}. \tag{2.12}$$

From these eigenstates we obtain the eigenstates of the rotated steady state by applying the rotation operator $\hat{R}(t)$,

$$|\phi_k(t)\rangle = \hat{R}(t)\,|v_k\rangle\,. \tag{2.13}$$

With the rotation operator $\hat{R}(t)$ having the form $e^{-i\omega t\hat{H}_1}$ we can now evaluate the terms containing the eigenstates in Eq. (1.41) as follows,

$$\langle\phi_k(0)|\phi_k(\tau)\rangle = \langle v_k|\,\hat{R}(0)\hat{R}(\tau)\,|v_k\rangle\,, \tag{2.14}$$

$$\left\langle \phi_k(t)\middle|\dot{\phi}_k(t)\right\rangle = -i\omega\,\langle v_k|\,\hat{H}_1\,|v_k\rangle\,. \tag{2.15}$$

Chapter 3

Applications

3.1 Mach-Zehnder-Interferometer Simulation

To check our results for the relative phases obtained in the systems we treat, we simulated the Mach-Zehnder interferometer introduced in Subsection 1.3.1. This simulation was done using the package *QuantumOptics* introduced in Appendix B and with the following choice of Hamiltonian,

$$\hat{H} = \hat{H}_S \otimes |1\rangle\langle 1|_B - \frac{\chi}{T}\hat{I}_S \otimes |0\rangle\langle 0|_B \,, \tag{3.1}$$

for the time evolution inbetween the two beam splitters. For details on the implementation, see Appendix B.1.

3.2 Qubit Pure Dephasing Dynamics

As a first application and as a way of testing our semi-analytical implementation of the formula for the geometric phase in non-adiabatic evolution, we consider the example of a Qubit subjected to pure dephasing. This system is also being treated in [17], in the following we extend the analytical solution presented there to initial conditions on the whole Bloch sphere. With the exact solution we can then perform tests of our semi-analytical implementation. The Qubit is subjected to the Hamiltonian,

$$\hat{H} = \Big(\frac{\eta}{2}\Big)\hat{\sigma}_z, \tag{3.2}$$

and experiences dephasing modeled by the Lindblad operator,

$$\hat{\Gamma} = \sqrt{\frac{\Lambda}{2}}\hat{\sigma}_z. \tag{3.3}$$

Here η is the precession rate and Λ the strength of dephasing. The given systems dynamics are governed by the QME,

$$\frac{\mathrm{d}}{\mathrm{d}t}\hat{\rho}(t) = -i\left[\omega\frac{\hat{\sigma}_z}{2}, \hat{\rho}(t)\right] + \frac{\Lambda}{2}\mathcal{D}[\hat{\sigma}_z]\hat{\rho}(t). \tag{3.4}$$

We start from an arbitrary pure state at time $t_0 = 0$ and parametrize the general solution of the time evolution as follows,

$$\hat{\rho}(t) = \frac{1}{2}\Big(\hat{I} + \vec{r}(t)\cdot\vec{\sigma}\Big), \tag{3.5}$$

where $\vec{r}(t) = (r_x(t), r_y(t), r_z(t))$ is the state-vector on the Bloch sphere and $\vec{\sigma} = (\hat{\sigma}_x, \hat{\sigma}_y, \hat{\sigma}_z)$ the Pauli vector. The coefficients of this parametrization are given by

$$\begin{aligned} r_x(t) &= e^{-\Lambda t}(r_x(0)\cos(\omega t) - r_y(0)\sin(\omega t)), \\ r_y(t) &= e^{-\Lambda t}(r_x(0)\sin(\omega t) - r_y(0)\cos(\omega t)), \\ r_z(t) &= r_z(0). \end{aligned} \tag{3.6}$$

The eigenvectors and eigenvalues of the density matrix are,

$$\lambda_\pm = \frac{1}{2}\left(1 \pm e^{-\Lambda t}\sqrt{r_x(0)^2 + r_y(0)^2 + e^{2\Lambda t} r_z(0)^2}\right),$$

$$|\psi_\pm(t)\rangle = \frac{1}{c}\begin{pmatrix} e^{-i\omega t}\frac{e^{\Lambda t} r_z(0) \pm \sqrt{r_x(0)^2 + r_y(0)^2 + e^{\Lambda t} r_z(0)^2}}{r_x(0) + i r_y(0)} \\ 1 \end{pmatrix}, \tag{3.7}$$

$$c = \sqrt{1 + \frac{\left(\pm e^{\Lambda t} r_z(0) + \sqrt{r_x(0)^2 + r_y(0)^2 + e^{\Lambda t} r_z(0)^2}\right)^2}{r_x(0)^2 + r_y(0)^2}}, \tag{3.8}$$

where $|0\rangle = \begin{pmatrix} 1 \\ 0 \end{pmatrix}$ and $|1\rangle = \begin{pmatrix} 0 \\ 1 \end{pmatrix}$. Using the polar decomposition

$$\begin{aligned} r_x(0) &= \sin(\theta_0)\cos(\varphi_0), \\ r_y(0) &= \sin(\theta_0)\sin(\varphi_0), \\ r_z(0) &= \cos(\theta_0), \end{aligned} \tag{3.9}$$

these results can be recast into the following form,

$$\lambda_\pm = \frac{1}{2}\left(1 \pm \sqrt{\cos^2(\theta_0) + e^{-\Lambda t}\sin^2(\theta_0)}\right), \tag{3.10}$$

$$|\psi_+\rangle = e^{i(\omega t + \varphi_0)/2}\cos\left(\frac{\theta_t}{2}\right)|1\rangle + e^{i(\omega t + \varphi_0)/2}\sin\left(\frac{\theta_t}{2}\right)|0\rangle, \tag{3.11}$$

$$|\psi_+\rangle = -e^{i(\omega t + \varphi_0)/2}\sin\left(\frac{\theta_t}{2}\right)|1\rangle + e^{i(\omega t + \varphi_0)/2}\cos\left(\frac{\theta_t}{2}\right)|0\rangle, \tag{3.12}$$

where

$$\theta_t = \left(\arctan\left(e^{-\Gamma t}\tan(\theta_0)\right) + \pi\right) \bmod \pi. \tag{3.13}$$

This result generalizes Eqs. (19) and (20) in [17]. We now turn to computing the geometric phase using Eq. (1.41). The overlap between the eigenstates and their time derivatives are:

$$\left\langle \psi_+(t)\middle|\dot{\psi}_+(t)\right\rangle = -i\frac{\omega}{2}\cos(\theta_0) = -i\frac{\omega}{2}\frac{1}{\sqrt{1 + e^{-\Lambda t}\tan^2(\theta_0)}}, \tag{3.14}$$

$$\left\langle \psi_-(t)\middle|\dot{\psi}_-(t)\right\rangle = i\frac{\omega}{2}\cos(\theta_0) = i\frac{\omega}{2}\frac{1}{\sqrt{1 + e^{-\Lambda t}\tan^2(\theta_0)}}. \tag{3.15}$$

Since $\lambda_-(t=0)=0$ we need only consider the terms corresponding to $|\psi_+\rangle$ in Eq. (1.41). Using the general formula,

$$\begin{aligned}\int_0^t \frac{1}{\sqrt{1+be^{-as}}}ds &= \left[\frac{2}{a}\text{artanh}\left(\frac{1}{\sqrt{1+be^{-as}}}\right)\right]_0^t \\ &= \left[\frac{1}{a}\ln\left(\frac{1+\frac{1}{\sqrt{1+be^{-as}}}}{1-\frac{1}{\sqrt{1+be^{-as}}}}\right)\right]_0^t,\end{aligned} \tag{3.16}$$

where we used $\text{artanh}(x)=\frac{1}{2}\ln\left((1+x)/(1-x)\right)$, we obtain,

$$e^{-\int_0^t\langle\psi_+(s))|\dot{\psi}_+(s)\rangle ds} = e^{i\frac{\eta}{4\Lambda}\ln\left(\frac{\left(\sqrt{\cos^2(\theta_0)+\sin^2(\theta_0)e^{-2\Lambda t}}\right)(1-\cos(\theta_0))}{\left(\sqrt{\cos^2(\theta_0)+\sin^2(\theta_0)e^{-2\Lambda t}}\right)(1+\cos(\theta_0))}\right)}, \tag{3.17}$$

such that Eq. (24) from [17] takes the form,

$$\begin{aligned}\gamma(t) =& \arg\left(e^{-i\frac{\eta}{2}t}\cos\left(\frac{\theta_t}{2}\right)\cos\left(\frac{\theta_0}{2}\right)+e^{i\frac{\eta}{2}t}\sin\left(\frac{\theta_t}{2}\right)\sin\left(\frac{\theta_0}{2}\right)\right) \\ &+\frac{\eta}{4\Lambda}\ln\left(\frac{\left(\sqrt{\cos^2(\theta_0)+\sin^2(\theta_0)e^{-2\Lambda t}}\right)(1-\cos(\theta_0))}{\left(\sqrt{\cos^2(\theta_0)+\sin^2(\theta_0)e^{-2\Lambda t}}\right)(1+\cos(\theta_0))}\right).\end{aligned} \tag{3.18}$$

For $t=T=\frac{2\pi}{\eta}$ this result simplifies to,

$$\begin{aligned}\gamma(T) =& \arg\left(\cos\left(\frac{\theta_T}{2}\right)\cos\left(\frac{\theta_T}{2}\right)+\sin\left(\frac{\theta_T}{2}\right)\sin\left(\frac{\theta_0}{2}\right)\right) \\ &+\frac{\eta}{4\Lambda}\ln\left(\frac{\left(\sqrt{\cos^2(\theta_0)+\sin^2(\theta_0)e^{-2\Lambda T}}\right)(1-\cos(\theta_0))}{\left(\sqrt{\cos^2(\theta_0)+\sin^2(\theta_0)e^{-2\Lambda T}}\right)(1+\cos(\theta_0))}\right),\end{aligned} \tag{3.19}$$

which, assuming $r_z(0)=\cos(\theta_0)\geq 0$ reduces to Eq. (21) of [17]. With the analytical formula for the geometric phase in this system we were able to benchmark our semi-analytical function. In all tested configurations for the parameters η, Λ and the initial conditions given by $\vec{r}(0)$ we observed quartic convergence. For an example see Fig. 3.1.

3.3 Van der Pol Spin One System

In this section we consider the van der Pol spin one system as an example of a dissipative quantum system exhibiting a limit cycle. As has been shown in [12], this system is the smallest system to exhibit a limit cycle in phase space. The van der Pol spin one system is described by the QME with the free Hamiltonian,

$$\hat{H}_0=\hbar\omega_0\hat{S}_z, \tag{3.20}$$

and the Lindblad operators,

$$\hat{\Gamma}_1=\sqrt{\frac{g_g}{2}}\left(\sqrt{2}\hat{S}_z\hat{S}_+-\hat{S}_+\hat{S}_z\right), \tag{3.21}$$

$$\hat{\Gamma}_2=\sqrt{\frac{g_d}{2}}\left(\hat{S}_-^2\right), \tag{3.22}$$

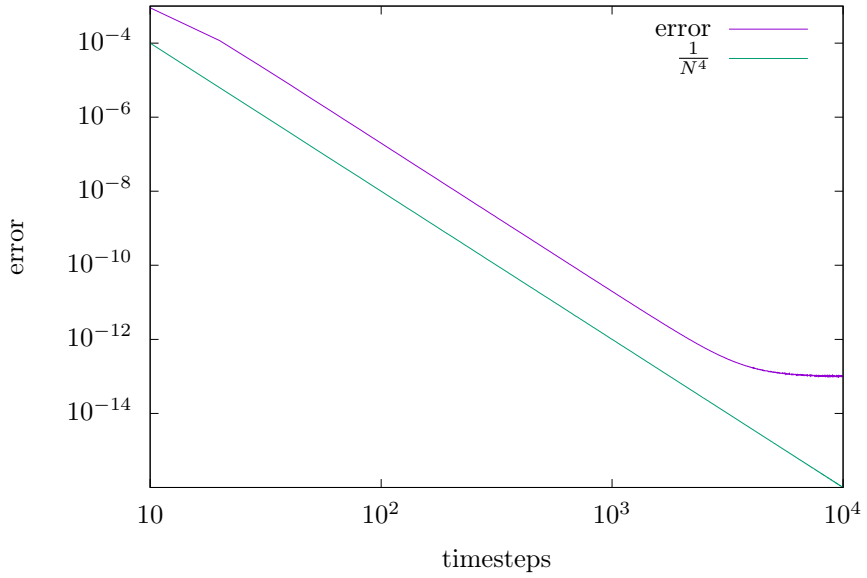

Figure 3.1: Convergence plot using our semi-analytical formula for the geometric phase compared to the analytical solution of the Qubit pure dephasing model. The parameters here were $\Lambda = 0.2,\ \eta = 1$ and the initial state was determined by $\theta_0 = \frac{\pi}{4},\ \varphi_0 = 0$.

following [7], where g_g is the gain rate and g_d the damping rate. To adiabatically change the free Hamiltonian $\hat{H}_0$ and the Lindblad operators we subject them to a rotation given by the rotation operator

$$\hat{R}(\alpha, t) = e^{-i\omega t \vec{n}(\alpha)\cdot\vec{S}}, \tag{3.23}$$

where $\vec{S} = (\hat{S}_x, \hat{S}_y, \hat{S}_z)^T$, $\vec{n}(\alpha) = (\sin(\alpha), 0, \cos(\alpha))$ and α the opening angle of the cone seen in Fig. 3.2. We cite the conditions for adiabatic changes of this system from [6],

$$\omega_0 \gg \omega, \tag{3.24}$$

as well as the conditions for the restriction of the van der Pol limit cycle oscillator to a three level system,

$$\omega_0 \gg g_d \gg g_g. \tag{3.25}$$

We further cite the steady state without rotation from [7],

$$\hat{\rho}_{\text{steady}} = \begin{pmatrix} \frac{g_g}{3g_d+g_g} & 0 & 0 \\ 0 & \frac{g_d}{3g_d+g_g} & 0 \\ 0 & 0 & \frac{2g_d}{3g_d+g_g} \end{pmatrix}, \tag{3.26}$$

which in the limit of $g_g \ll g_d$ simplifies to,

$$\hat{\rho}_{\text{steady}} \to \begin{pmatrix} 0 & 0 & 0 \\ 0 & \frac{1}{3} & 0 \\ 0 & 0 & \frac{2}{3} \end{pmatrix}. \tag{3.27}$$

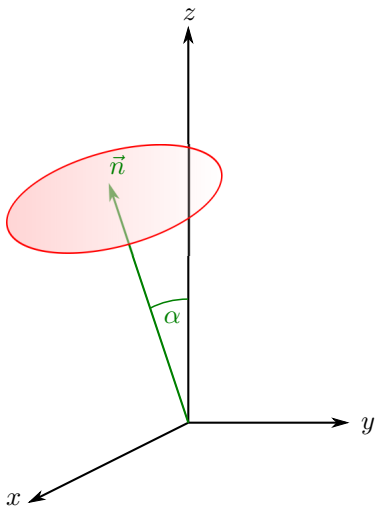

Figure 3.2: Visualization of the rotation that we subject the van der Pol system to.

Analytical approach

Using the method explained in Subsection 2.2.1, we found the approximate steady state of the system in the rotating frame by setting both equations in Eq. (2.9) to zero. For $\hat{\chi}^{(0)}_{\text{steady}}$ we recover the steady state for the non-rotating system,

$$\hat{\chi}^{(0)}_{\text{steady}} = \hat{\rho}_{\text{steady}} = \begin{pmatrix} \frac{g_g}{3g_d+g_g} & 0 & 0 \\ 0 & \frac{g_d}{3g_d+g_g} & 0 \\ 0 & 0 & \frac{2g_d}{3g_d+g_g} \end{pmatrix}, \tag{3.28}$$

and for the second coefficient in the perturbation series we get,

$$\hat{\chi}^{(1)}_{\text{steady}} = \begin{pmatrix} 0 & a & 0 \\ a^* & 0 & b \\ 0 & b^* & 0 \end{pmatrix}, \tag{3.29}$$

with

$$a = \frac{\left(i(4+3\sqrt{2})g_g g_d - 2\sqrt{2}g_g\omega_0 + \sqrt{2}g_g(2\omega_0 - 3ig_g)\right)}{2(3g_d+g_g)(g_d+g_g+i\omega_0)(3g_g+2i\omega_0)}, \tag{3.30}$$

$$b = \frac{i\sqrt{2}g_d \sin(\alpha)}{(3g_d+g_g)(3g_g+2i\omega_0)}. \tag{3.31}$$

For small values of ω we have

$$\hat{\chi}_{\text{steady}} \approx \hat{\chi}^{(0)} + \omega\hat{\chi}^{(1)} = \begin{pmatrix} \frac{g_g}{3g_d+g_g} & \omega a & 0 \\ \omega a^* & \frac{g_d}{3g_d+g_g} & \omega b \\ 0 & \omega b^* & \frac{2g_d}{3g_d+g_g} \end{pmatrix}, \tag{3.32}$$

and by applying the rotation we can get the rotated steady state,

$$\hat{\rho}_{\text{steady}}(t,\alpha) = \hat{R}(\alpha,t)\hat{\chi}_{\text{steady}}\hat{R}^\dagger(\alpha,t). \tag{3.33}$$

Our evolution is adiabatic, so for small ω takes place during long time intervals compared to the systems inherent dynamics. Therefore we can assume that the systems stays in its steady state during the rotation and we take $\hat{\rho}_{\text{steady}}$ as a reasonable approximation to the systems state during its evolution. With this assumption we can now evaluate Eq. (1.41) analytically. Considering the eigenvalues and eigenstates of $\hat{\chi}_{\text{steady}}$ as close to the eigenvalues and eigenstates of $\hat{\chi}^{(0)}$ we employ perturbation theory again to find the following approximation to first order,

$$w_1 = w_1^{(0)},\ w_0 = w_0^{(0)},\ w_{-1} = w_{-1}^{(0)}, \tag{3.34}$$

$$v_1 \approx v_1^{(0)} + \begin{pmatrix} 0 \\ \frac{\omega(i(4+3\sqrt{2})g_d g_g + \sqrt{2}g_g(-3ig_g - 2\omega_0) + 2\sqrt{2}g_d\omega_0)\sin(\alpha)}{2(g_d - g_g)(g_d + g_g - i\omega_0)(3g_g - 2i\omega_0)} \\ 0 \end{pmatrix}, \tag{3.35}$$

$$v_0 \approx v_0^{(0)} + \begin{pmatrix} \frac{\omega(i(4+3\sqrt{2})g_d g_g - 2\sqrt{2}g_d\omega_0 + \sqrt{2}g_g(-3ig_g + 2\omega_0))\sin(\alpha)}{2(g_d - g_g)(g_d + g_g + i\omega_0)(3g_g + 2i\omega_0)} \\ 0 \\ -\frac{\sqrt{2}\omega\sin(\alpha)}{3ig_g + 2\omega_0} \end{pmatrix}, \tag{3.36}$$

$$v_{-1} \approx v_{-1}^{(0)} + \begin{pmatrix} 0 \\ \frac{i\sqrt{2}\omega\sin(\alpha)}{3g_g + 2i\omega_0} \\ 0 \end{pmatrix}. \tag{3.37}$$

Here the w_k are the eigenvalues and v_k the eigenstates of $\hat{\chi}_{\text{steady}}$ in the rotating frame and $v_k^{(0)}$ the k-th canonical basis vector in $\mathbb{R}^3$. Rotating the eigenstates yields the eigenstates of $\hat{\rho}_{\text{steady}}(t, \alpha)$ and with these we evaluate Eq. (1.41) as outlined in Subsection 2.2.1 to find a perturbative approximation to the geometric phase γ_{perturb}. The full solution is rather long and intransparent, we therefore consider the limiting case of no interaction to the environment,i.e. $g_g = g_d = 0$,

$$\gamma_{\text{perturb.}} = \tag{3.38}$$
$$\arg\left(\frac{1}{3} + \frac{2}{3}e^{2\pi i\left(\cos(\alpha) - \frac{\omega\sin^2(\alpha)}{\omega_0}\right)} + \left(\frac{\omega\sin(\alpha)}{\omega_0}\right)^2\left(1 + e^{2\pi i\left(\cos(\alpha) - \frac{\omega\sin^2(\alpha)}{\omega_0}\right)}\right)\right),$$

and the case where the rotation frequency ω tends to zero,

$$\gamma_{\text{perturb.}} = \arg\left(\frac{g_d}{3g_d + g_g} + \frac{2g_d e^{2i\pi\cos(\alpha)}}{3g_d + g_g} + \frac{g_g e^{-2i\pi\cos(\alpha)}}{3g_d + g_g}\right). \tag{3.39}$$

3.3.1 Closed System

We first treat the spin one system without interaction to the environment by setting the gain rate g_g and damping rate g_d of our model to zero. Therefore we effectively consider the rotated free Hamiltonian,

$$\hat{H}(\alpha, t) = \hat{R}(\alpha, t)\hat{H}_0\hat{R}(\alpha, t)^\dagger. \tag{3.40}$$

From the eigenstates of the free Hamiltonian $\hat{H}_0$ we get the eigenstates of the rotated Hamiltonian $\hat{H}(\alpha, t)$ by simply applying the rotation,

$$|\phi_1(\alpha,t)\rangle = \begin{pmatrix} \left(\cos\left(\frac{t\omega}{2}\right) - i\cos(\alpha)\sin\left(\frac{t\omega}{2}\right)\right)^2 \\ -\sqrt{2}\sin(\alpha)\sin\left(\frac{t\omega}{2}\right)\left(i\cos\left(\frac{t\omega}{2}\right) + \cos\left(\alpha\sin\left(\frac{t\omega}{2}\right)\right)\right) \\ -\sin(\alpha)^2\sin\left(\frac{t\omega}{2}\right)^2 \end{pmatrix},$$

$$|\phi_0(\alpha,t)\rangle = \begin{pmatrix} -\sqrt{2}\sin(\alpha)\sin\left(\frac{t\omega}{2}\right)\left(i\cos\left(\frac{t\omega}{2}\right) + \cos(\alpha)\sin\left(\frac{t\omega}{2}\right)\right) \\ \cos(\alpha)^2 + \cos(t\omega)\sin(\alpha)^2 \\ \sqrt{2}\sin(\alpha)\sin\left(\frac{t\omega}{2}\right)\left(-i\cos\left(\frac{t\omega}{2}\right) + \cos(\alpha)\sin\left(\frac{t\omega}{2}\right)\right) \end{pmatrix},$$

$$|\phi_{-1}(\alpha,t)\rangle = \begin{pmatrix} -\sin(\alpha)^2\sin\left(\frac{t\omega}{2}\right)^2 \\ \sqrt{2}\sin(\alpha)\sin\left(\frac{t\omega}{2}\right)\left(-i\cos\left(\frac{t\omega}{2}\right) + \cos(\alpha)\sin\left(\frac{t\omega}{2}\right)\right) \\ \left(\cos\left(\frac{t\omega}{2}\right) + i\cos(\alpha)\sin\left(\frac{t\omega}{2}\right)\right)^2 \end{pmatrix}.$$

From these we can find the Berry phase of each eigenstate using the formula for the pure state geometric phase introduced in Subsection 1.2.1,

$$\gamma_k(\alpha,t) = i\int_0^t \langle\phi_k(\alpha,s)|\dot{\phi_k}(\alpha,s)\rangle\, ds, \tag{3.41}$$

which for one closed loop, i.e. $t = \dfrac{2\pi}{\omega}$, yields,

$$\gamma_k(\alpha) = 2\pi(1-\cos(\alpha))\cdot k, \tag{3.42}$$

where $k \in \{+1, 0, -1\}$. During adiabatic evolution the initial mixed state $\hat{\rho}_{\text{steady}}$ stays diagonal in the basis of the rotating Hamiltonian and we can therefore compute its geometric phase from the geometric phases of each eigenstate as shown in [15]:

$$\gamma = \arg\left(\sum_k w_k e^{i\gamma_k}\right) = \arg\left(\frac{1}{3} + \frac{2}{3}e^{-2\pi i(1-\cos(\alpha))}\right), \tag{3.43}$$

for the steady state from Eq. (3.27) as initial state and where w_k are the diagonal entries of the initial state. With the same assumptions on adiabaticity, evaluating Eq. (1.41) analytically yields the same result. The analytical solution obtained through perturbation theory for finite ω reduces to the formula given in Eq. (3.38) for $g_g, g_d \to 0$. Lastly we can compute the geometric phase using our semi-analytical formula. Results for all three approaches are shown in Fig. 3.3. The expression for the interference pattern in the interferometer follows from the material described in Subsection 1.3.1,

$$\begin{aligned} p_0 &= \langle 0|_B \operatorname{Tr}_S(\hat{\rho}_{\text{out}})\,|0\rangle_B = \frac{1}{2}(1+\nu\cos(\chi-\gamma)), \\ p_1 &= \langle 1|_B \operatorname{Tr}_S(\hat{\rho}_{\text{out}})\,|1\rangle_B = \frac{1}{2}(1-\nu\cos(\chi-\gamma)), \end{aligned} \tag{3.44}$$

where ν is the visibility given by $\nu = \left|\sum_k w_k e^{i\gamma_k}\right|$. The observed relative phase equals the geometric phase here since we are evolving our system adiabatically for small ω and since the time evolution is chosen such that the dynamical phase vanishes.

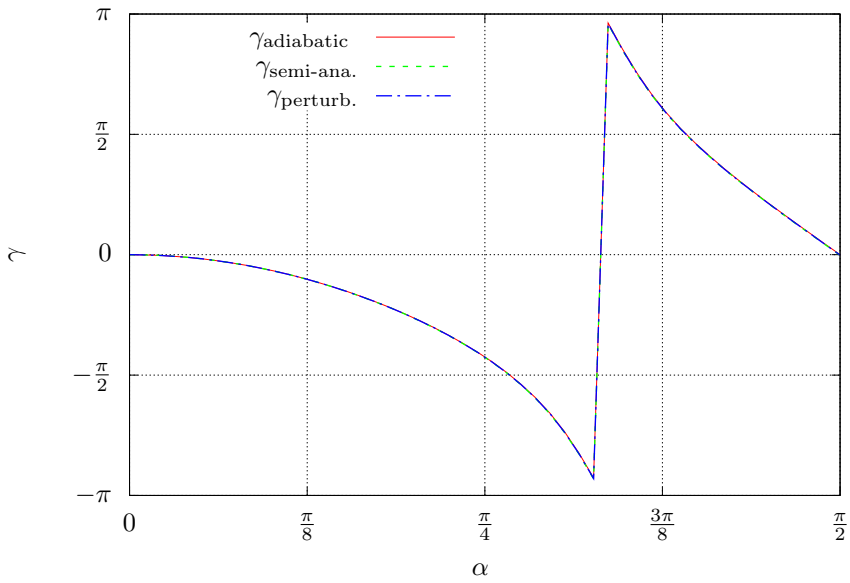

Figure 3.3: The GP in the closed case for $\omega = 0.001$ and three different approaches. $\gamma_{\text{adiabatic}}$ is obtained using Eq. (3.43) or equivalently by evaluating Eq. (1.41) in the adiabatic limit and $\gamma_{\text{semi-ana.}}$ is the result of our semi-analytical implementation of Eq. (1.41). $\gamma_{\text{perturb.}}$ is calculated with the perturbative solution from Eq. (3.38) of the GP for finite ω.

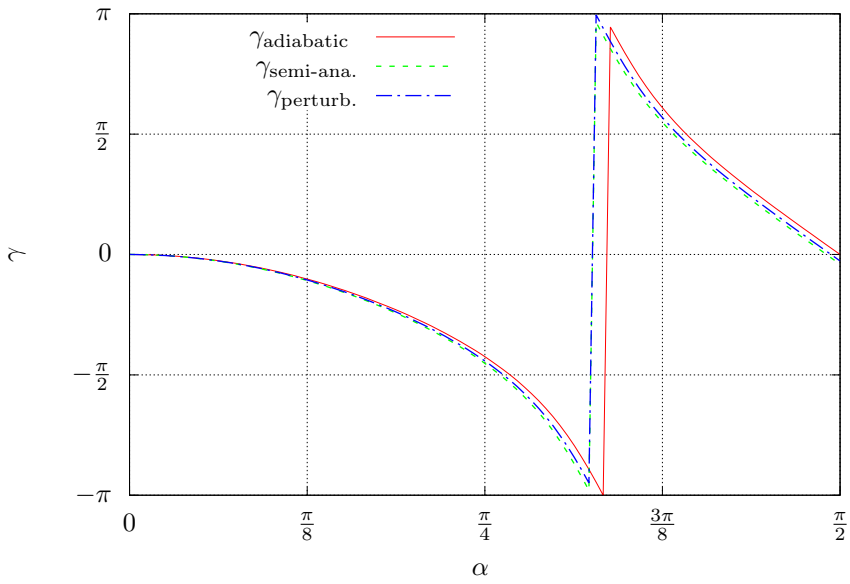

Figure 3.4: GP in the closed case for $\omega = 0.02$ and three different approaches. $\gamma_{\text{adiabatic}}$ is obtained using Eq. (3.43) or equivalently by evaluating Eq. (1.41) in the adiabatic limit and $\gamma_{\text{semi-ana.}}$ is the result of our semi-analytical implementation of Eq. (1.41). $\gamma_{\text{perturb.}}$ is calculated with the perturbative solution from Eq. (3.38) of the GP for finite ω. As can be expected from Eq. (3.38), the corrections to the GP get larger for larger values of α.

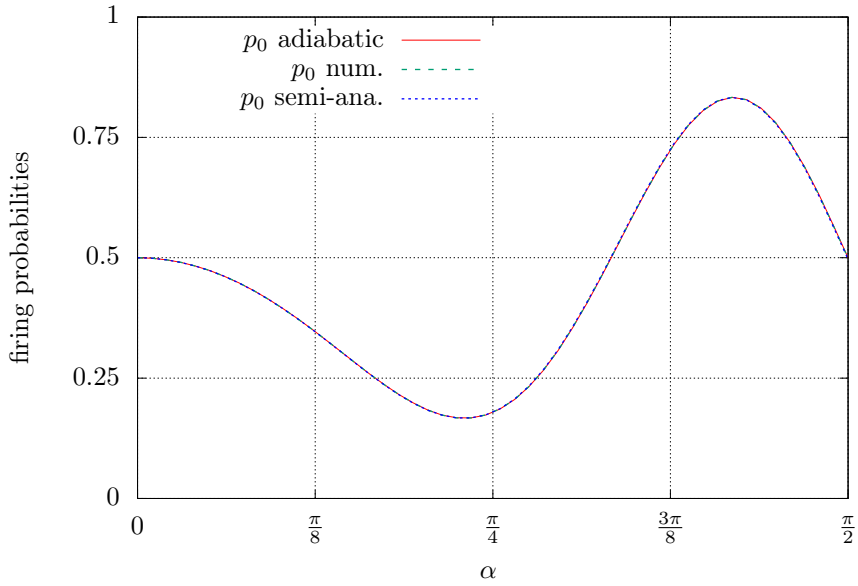

Figure 3.5: Firing probabilities of the MZI for $\omega = 0.001$, $\omega_0 = 1$ and $\chi = \frac{\pi}{2}$. The analytical firing probabilities are computed using Eq. (3.44) and the steady state given in Eq. (3.27). The numerical firing probabilites are computed using the simulation of the MZI with the same input state.

3.3.2 Open System

We now consider the general case of the van der Pol spin one system where the gain rate g_g and the damping rate g_d are no longer zero. In effect this means we switch on coupling to the environment, modeled by the Lindblad operators from Eq. (3.22). Here we rely on our perturbative solution to confirm the result of our semi-analytical formula for small values of ω. As explained in Subsection 1.3.2, an extension of the interferometric measurement to the case of non-unitary evolution is only possible with the ancilla system. In effect this means performing an interferometeric measurement of a pure state where the van der Pol system would be part of a subspace. We therefore restrict ourselves to determining the geometric phase of the open system here. For an in-depth discussion of the intereferometric measurement with non-unitary evolution and especially with the system considered here, see Appendix A.

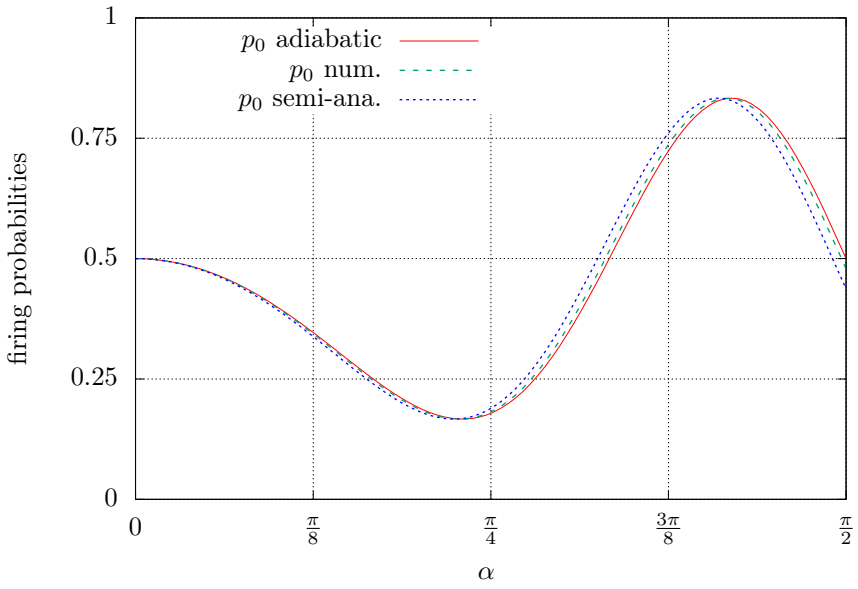

Figure 3.6: Firing probabilities of the MZI in the closed case for $\omega = 0.02$, $\omega_0 = 1$ and $\chi = \frac{\pi}{2}$. The analytical firing probabilities are computed using Eq. (3.44) and the steady state given in Eq. (3.27). The numerical firing probabilites are computed using the simulation of the MZI with the same input state. The discrepancy between the numerical result and the one predicted by the semi-analytical approach is due to the different eigenbasis for nonzero ω leading to the dynamical phase no longer being a multiple of 2π. This could be compensated by adjusting the time evolution.

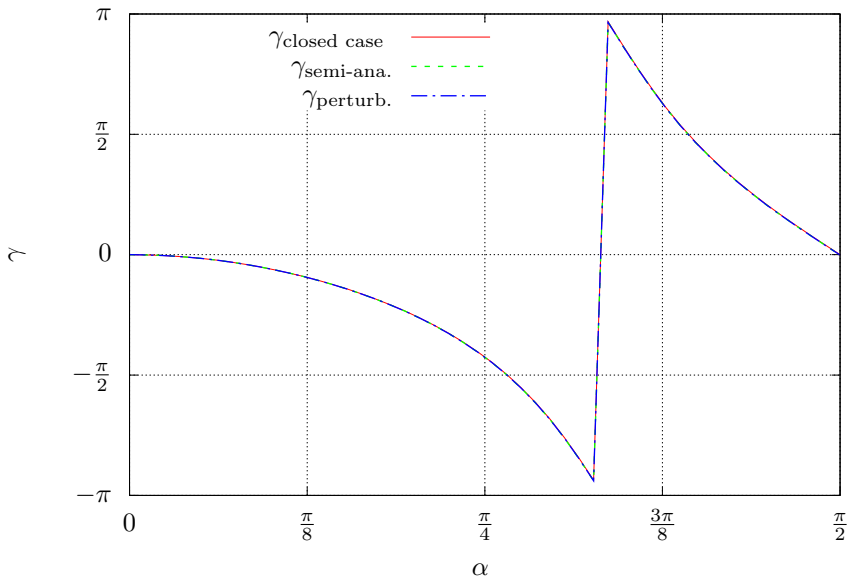

Figure 3.7: GP in the open case with $\omega = 0.001$, $\omega_0 = 1$ and $\chi = \frac{\pi}{2}$. The coupling rates are $g_g = 0.001$ and $g_d = 0.01$. We see that the GP does not change significantly with respect to the closed case.

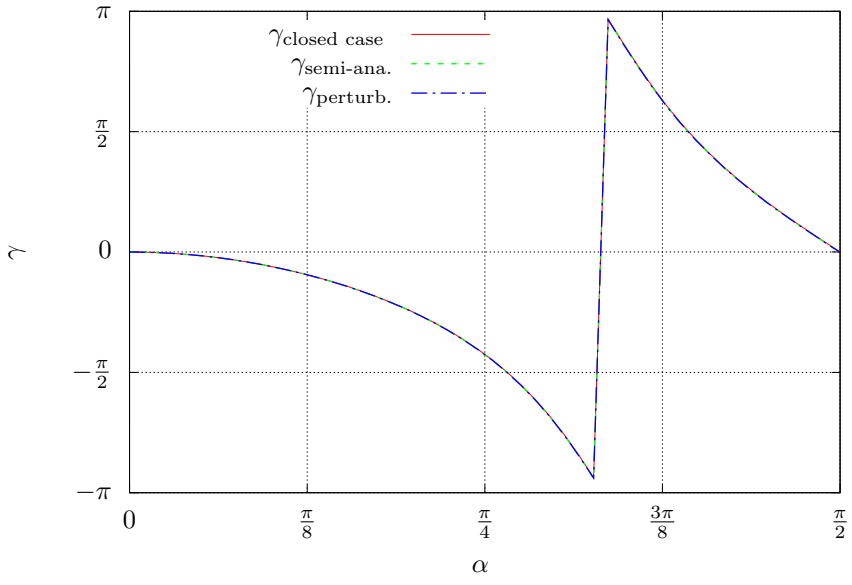

Figure 3.8: GP in the open case with $\omega = 0.001$, $\omega_0 = 1$ and $\chi = \frac{\pi}{2}$. The coupling rates are $g_g = 0.01$ and $g_d = 0.1$. We again see that the GP does not change significantly with respect to the closed case.

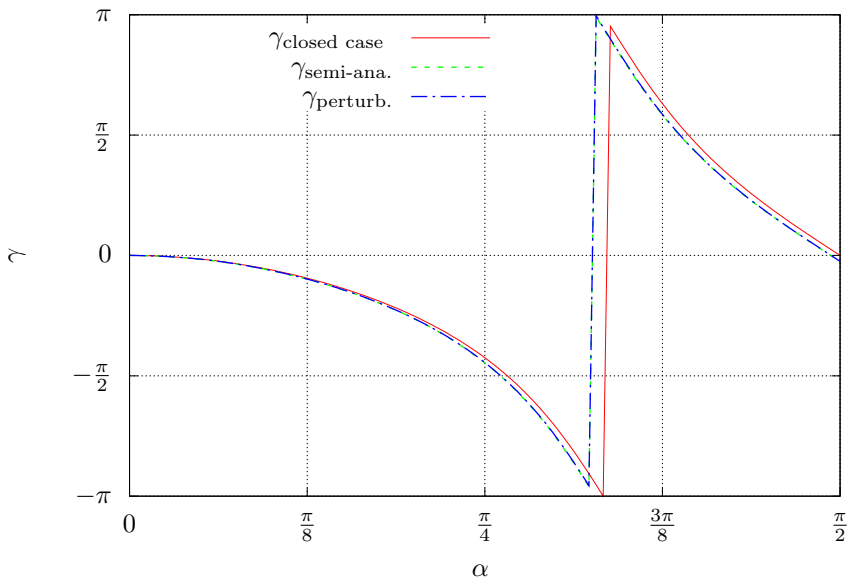

Figure 3.9: GP in the open case with $\omega = 0.02$, $\omega_0 = 1$ and $\chi = \frac{\pi}{2}$. The coupling rates are $g_g = 0.01$ and $g_d = 0.1$. Here the perturbative solution and the semi-analytical solution agree even better than in the closed case, see Fig. 3.4. This is due to the nonzero gain- and damping rates pushing the system faster into its steady state upon which the perturbative approach relies.

Conclusion

In this thesis we laid out the basic theory of quantum geometric phases for both pure states and mixed states. The latter case was needed for our treatment of non-unitary processes such as the van der Pol spin one system. Since the problem we wanted to treat, i.e. the van der Pol spin one system, proved not to be analytically solvable we developed a semi-analytical approach to evaluating the general formula for the geometric phase in non-unitary evolution given in [17]. This approach was based on solving the QME describing our system through the use of the *QuantumOptics* package in Julia and subsequent numerical calculations. We tested this approach with the analytically solvable example from [17] and slightly extended the analytical solution to arbitrary inital conditions. Our semi-analytical formula showed quartic convergence in all tested regions of the parameter space which was to be expected given the accuracy of the employed numerical procedures. Turning to the van der Pol spin one system we first considered the limiting case of no interaction to the environment and were able to analytically derive the geometric phase of this system, both using the approach of [15] and the general formula given in [17] in the adiabatic limit. This analytical result agreed well with our semi-analytical implementation of the general formula from [17] and we were able to produce the expected interference pattern explained in [15] for small rotation frequencies in our simulation of the MZI. We investigated the problems that led to the geometric phase not being computed correctly for the open case in [6] and found out that besides numerical problems the geometric phase in that case is generally not measurable with the employed interferometric setup. With our semi-analytical formula, as well as with an approximate solution obtained through perturbation theory, we were able to show that the geometric phase in the open case stays close to the one from the closed case for small gain and damping rates, see Fig. 3.7, and is well predicted by our semi-analytical formula. We also derived a formula to predict the interference pattern of the Mach-Zehnder interferometer in the case of non-zero dissipation. After realizing that the geometric phase in non-unitary evolution is in general not measurable in this way we discontinued work in that direction, the results can be found in Appendix A. We finish the endeavour of showing that a quantum limit-cycle system reveals a geometric phase with two new insights. For one we found that this phase is in general not measurable in the envisaged way through a Mach-Zehnder interferometer. On the other side we are confident that the van der Pol spin one system, prepared in its steady state and with its quantization axis slowly rotated attains a geometric phase that also persists with finite gain and damping rates as long as adiabaticity is retained.

Appendix A

Interferometry in the Non-Unitary Case

Trying to extend the measurements of the geometric phase into the case of non-unitary evolution fails in our case. The proposed method of measuring the geometric phase in this case from [17] uses the purified state Ψ for the interference measurement and does not work with the mixed state $\hat{\rho}_S$ itself. In this chapter we present our understanding of the interference pattern of the Mach-Zehnder interferometer in the case of nonzero gain and damping rates.

A.1 Interference Pattern

In an effort to understand the interference pattern produced in the case of non-unitary evolution of the internal system we derived expressions for the visibility and phase shift generalizing the ones given in Subsection 1.3.1. We consider the Hilbert space of the beam $\mathcal{H}_B = \{|0\rangle_B, |1\rangle_B\}$ and the Hilbert space of an additional system $\mathcal{H}_S = \{|n\rangle_S\}_n$ together in a combined Hilbert space $\mathcal{H}_B \otimes \mathcal{H}_S$. States that go into the Mach-Zehnder interferometer therefore have an additional degree of freedom described by $\mathcal{H}_S$ and two possible polarizations. In the cases we investigated, the evolution of the system in its own Hilbert space is governed by a QME of the following form,

$$\frac{\mathrm{d}}{\mathrm{d}t}\hat{\rho}_S(t) = -i\Big[\hat{H}_S(t), \hat{\rho}_S(t)\Big] + \sum_i \mathcal{D}\Big[\hat{\Gamma}_{S_i}(t)\Big]\hat{\rho}_S(t), \tag{A.1}$$

for a given Hamiltonian $\hat{H}_S(t)$ and Lindblad operators $\hat{\Gamma}_S(t)$. The beam only experiences a phase shift given by

$$\hat{U}_{PS_B} = e^{i\chi}\,|0\rangle\langle 0|_B + |1\rangle\langle 1|_B\,. \tag{A.2}$$

We now lift these operations from $\mathcal{H}_S$ and $\mathcal{H}_B$ into the combined space $\mathcal{H}_B \otimes \mathcal{H}_S$, with the systems evolution taking place in the upper arm of the interferometer

and the phase shift taking place in the lower arm.

$$\hat{U}_{M_B} \to \hat{U}_{M_B} \otimes \hat{I}_S := \hat{U}_M,\ \hat{U}_{BS_B} \to \hat{U}_{BS_B} \otimes \hat{I}_S := \hat{U}_{BS}. \tag{A.3}$$

$$\hat{H}(t) = |1\rangle\langle 1|_B \otimes \hat{H}_S(t) - \frac{\chi}{T}|0\rangle\langle 0|_B \otimes \hat{I}_S, \tag{A.4}$$

$$\hat{\Gamma}_{S_i}(t) \to |1\rangle\langle 1|_B \otimes \hat{\Gamma}_{S_i}(t) := \hat{\Gamma}_i(t),\ \hat{\rho}(t) = \hat{\rho}_B(t) \otimes \hat{\rho}_S(t). \tag{A.5}$$

Now the time evolution of the whole system in between the two beam-splitters is governed by the following QME,

$$\frac{\mathrm{d}}{\mathrm{d}t}\hat{\rho}(t) = -i\Big[\hat{H}(t), \hat{\rho}(t)\Big] + \sum_i \mathcal{D}\Big[\hat{\Gamma}_i(t)\Big]\hat{\rho}(t). \tag{A.6}$$

To find an expression for the phase shift α observed with the visibility ν we look at a general state going into the interferometer given as follows,

$$\hat{\rho}_0 = \hat{\rho}_{0_B} \otimes \hat{\rho}_{0_S} = |0\rangle\langle 0|_B \otimes \hat{\rho}_{0_S}. \tag{A.7}$$

Through the first beam splitter this state transforms into

$$\hat{\rho}_1 = \hat{U}_{BS}\,\hat{\rho}_0\,\hat{U}_{BS}^\dagger = \frac{1}{2}(|0\rangle\langle 0|_B + |0\rangle\langle 1|_B + |1\rangle\langle 0|_B + |1\rangle\langle 1|_B) \otimes \hat{\rho}_{0_S}. \tag{A.8}$$

Between the two beam splitters, the beam system does not undergo any change so we can plug $\frac{1}{2}(|0\rangle\langle 0|_B + |0\rangle\langle 1|_B + |1\rangle\langle 0|_B + |1\rangle\langle 1|_B) \otimes \hat{\rho}_Q(t)$ into the QME to obtain the time evolution. This yields the subsequent equation where we assumed the existence of only one Lindblad operator $\hat{\Gamma}_S$ for notational purpose,

$$\begin{aligned}
\frac{\mathrm{d}}{\mathrm{d}t}\hat{\rho}(t) = &\frac{i}{2}\ (|0\rangle\langle 1|_B + |1\rangle\langle 1|_B) \otimes \hat{\rho}_S(t)\hat{H}_S(t) \\
&- \frac{i}{2}(|1\rangle\langle 0|_B + |1\rangle\langle 1|_B) \otimes \hat{H}_S(t)\hat{\rho}_S(t) \\
&+ \frac{i\chi}{2T}((|0\rangle\langle 1|_B - |1\rangle\langle 0|_B \otimes \hat{\rho}_S(t))) + \frac{1}{2}\Big(|1\rangle\langle 1|_B \otimes \hat{\Gamma}_S\hat{\rho}_S(t)\hat{\Gamma}_S^\dagger\Big) \\
&- \frac{1}{4}((|1\rangle\langle 1|_B + |1\rangle\langle 0|_B) \otimes \hat{\Gamma}_S^\dagger\hat{\Gamma}_S\hat{\rho}_S(t) \\
&+ (|1\rangle\langle 1|_B + |0\rangle\langle 1|_B) \otimes \hat{\rho}_S(t)\hat{\Gamma}_S^\dagger\hat{\Gamma}_S),
\end{aligned} \tag{A.9}$$

which we rearrange to,

$$\begin{aligned}
\frac{\mathrm{d}}{\mathrm{d}t}\hat{\rho}(t) = &- |1\rangle\langle 0|_B \otimes \frac{i}{2}\underbrace{\left(\hat{H}_S + \frac{\chi}{T}I - \frac{i}{2}\hat{\Gamma}_S^\dagger\hat{\Gamma}_S\right)}_{:=\hat{H}_{eff}}\hat{\rho}_S(t) \\
&+ |0\rangle\langle 1|_B \otimes \frac{i}{2}\hat{\rho}_S(t)\underbrace{\left(\hat{H}_S + \frac{\chi}{T}\hat{I} + \frac{i}{2}\hat{\Gamma}_S^\dagger\hat{\Gamma}_S\right)}_{=\hat{H}_{eff}^\dagger} \\
&+ |1\rangle\langle 1|_B \otimes \frac{1}{2}\underbrace{\Big(-i\Big[\hat{H}_S(t), \hat{\rho}_S(t)\Big] + \mathcal{D}\Big[\hat{\Gamma}_S\Big]\Big)}_{:=\hat{\mathcal{L}}\hat{\rho}_S(t)}\hat{\rho}_S(t) \\
= &\frac{1}{2}\Big(-i\,|1\rangle\langle 0|_B \otimes \hat{H}_{eff}\hat{\rho}_S(t) + i\,|0\rangle\langle 1|_B \otimes \hat{\rho}_S(t)\hat{H}_{eff}^\dagger + |1\rangle\langle 1|_B \otimes \hat{\mathcal{L}}\hat{\rho}_S(t)\Big).
\end{aligned} \tag{A.10}$$

Having introducted the effective Hamiltonian $\hat{H}_{\text{eff}}$ and the Lindbladian $\hat{\mathcal{L}}$ we can formaly solve the time evolution for a time independent Hamiltonian by defining $\hat{U}_{\text{eff}}$,

$$\hat{U}_{\text{eff}}(t) = e^{-i\hat{H}_{\text{eff}}t} = e^{-i\chi\frac{t}{T}} e^{-i\hat{H}_S t - \frac{1}{2}\hat{\Gamma}_S^\dagger \hat{\Gamma}_S t} =: e^{-i\chi\frac{t}{T}} \hat{U}(t), \tag{A.11}$$

as the effective time evolution operator. With this we get the formal solution for the state inbetween the two beam-splitters,

$$\begin{aligned}\hat{\rho}_2(t) = {} & |1\rangle\langle 1|_B \otimes e^{\hat{\mathcal{L}}t}\hat{\rho}_{0_S} \\ & + |0\rangle\langle 0|_B \otimes \hat{\rho}_{0_S} + |1\rangle\langle 0|_B \otimes \hat{U}_{\text{eff}}(t)\hat{\rho}_{0_S} + |0\rangle\langle 1| \otimes \hat{\rho}_{0_S}\hat{U}_{\text{eff}}^\dagger(t).\end{aligned} \tag{A.12}$$

To obtain the state exiting the interferometer we have to apply the operator of the beam-splitter again,

$$\begin{aligned}\hat{\rho}_3(t) &= \hat{U}_{BS}\,\hat{\rho}_2(t)\,\hat{U}_{BS}^\dagger \\ &= \frac{1}{2}((|0\rangle\langle 0|_B - |0\rangle\langle 1|_B - |1\rangle\langle 0|_B + |1\rangle\langle 1|_B) \otimes e^{\hat{\mathcal{L}}t}\hat{\rho}_{0_S} \\ &\quad + (|0\rangle\langle 0|_B + |0\rangle\langle 1|_B + |1\rangle\langle 0|_B) + |1\rangle\langle 1|_B) \otimes \hat{\rho}_{0_S} \\ &\quad + (|0\rangle\langle 0|_B + |0\rangle\langle 1|_B - |1\rangle\langle 0|_B - |1\rangle\langle 1|_B) \otimes \hat{U}_{\text{eff}}(t)\hat{\rho}_{0_S} \\ &\quad + (|0\rangle\langle 0|_B - |0\rangle\langle 1|_B + |1\rangle\langle 0|_B - |1\rangle\langle 1|_B) \otimes \hat{\rho}_{0_S}\hat{U}_{\text{eff}}^\dagger(t))).\end{aligned} \tag{A.13}$$

With this we can now calculate the firing probability of a detector at the horizontal position p_0 or a detector at the vertical position p_1:

$$\begin{aligned}p_0 &= \langle 0|_B \,\text{tr}(\hat{U}_{BS}\hat{\rho}(t)\hat{U}_{BS}^\dagger)\,|0\rangle_B = \text{tr}\Big(e^{\hat{\mathcal{L}}t}\hat{\rho}_{0_S} + \hat{\rho}_{0_S} + \hat{U}_{\text{eff}}(t)\hat{\rho}_{0_S} + \hat{\rho}_{0_S}\hat{U}_{\text{eff}}^\dagger(t)\Big) \\ &= \text{tr}(e^{\hat{\mathcal{L}}t}\hat{\rho}_{0_S}) + \text{tr}(\hat{\rho}_{0_S}) + \text{tr}(\hat{U}_{\text{eff}}(t)\hat{\rho}_{0_S}) + \text{tr}(\hat{\rho}_{0_S}\hat{U}_{\text{eff}}^\dagger(t)),\end{aligned} \tag{A.14}$$

$$p_1 = 1 - p_0. \tag{A.15}$$

We recall the following useful identity which is a consequence of the QME preserving the trace,

$$\text{tr}(\hat{\mathcal{L}}\hat{\rho}) = 0. \tag{A.16}$$

This helps us to find,

$$\text{tr}_S(e^{\hat{\mathcal{L}}t}\hat{\rho}_{0_S}) = \sum_{k=0}^{\infty} \frac{t^k}{k!}\text{tr}_S(\hat{\mathcal{L}}^k\hat{\rho}_{0_S}) = 1. \tag{A.17}$$

Further using that $\text{tr}(\hat{\rho}_{0_S}\hat{U}_{\text{eff}}^\dagger(t)) = \text{tr}\Big(\hat{U}_{\text{eff}}(t)\hat{\rho}_{0_S}\Big)^*$, we arrive at the final form,

$$p_0 = \frac{1}{2}\left(1 + \nu\cos\left(\chi\frac{t}{T} - \alpha\right)\right), \tag{A.18}$$

with $\nu = |\text{tr}_S(\hat{U}(t)\hat{\rho}_{0_S})|$ and $\alpha = \arg(\text{tr}_S(\hat{U}(t)\hat{\rho}_{0_S}))$. Using these formulas we are now able to predict the interference pattern resulting from interferometric measurements involving non-unitary evolution in the upper arm. For the van

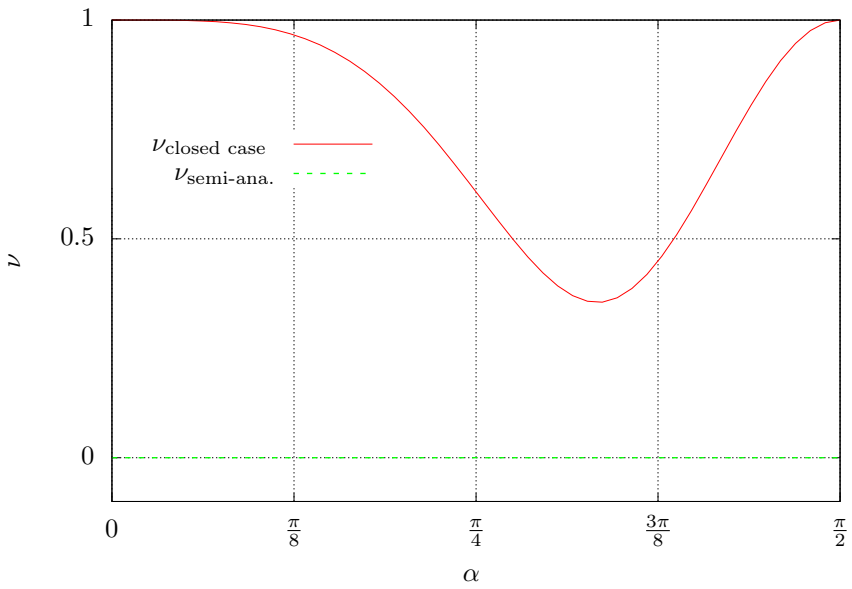

Figure A.1: Visibility of the interference pattern in the MZI for $\omega = 0.001$, $\omega_0 = 1$ and $\chi = \frac{\pi}{2}$, $g_g = 0.01$ and $g_d = 0.1$ compared to the visibility in the closed case. For this particular combination of parameters the visibility of the interference pattern in the open case tends to zero, effectively making a detection of the geometric phase with this setup impossible.

der Pol spin one system without rotation the effective unitary operator is the following,

$$\hat{U}_{\text{eff}}(T) = e^{-i\chi\hat{I} - i\hat{H}_0 T - \frac{1}{2}(\hat{\Gamma}_1^\dagger\hat{\Gamma}_1 + \hat{\Gamma}_2^\dagger\hat{\Gamma}_2)T}, \tag{A.19}$$

with the Lindblad operators $\hat{\Gamma}_1, \hat{\Gamma}_2$ and the Hamiltonian $\hat{H}_0$ from Section 3.3. One finds that thus the visibility decays proportional to $e^{-\min(g_g, g_d)\,T}$. So for large damping- and gain rates or equivalently for long times T the visibility of the interference pattern goes to zero. For an example see Fig. A.3.

A.1.1 Time-dependent Hamiltonian

We now continue the calculation above for the case of a time-dependent Hamiltonian $\hat{H}_S(t)$. This will be necessary for the treatment of the Van der Pol spin one system where the spin quantization axis is slowly rotated. We divide up the time axis from zero to t into N equal subintervals, each of length

$$\varepsilon = \frac{t}{N}.$$

The effective time-evolution operator is then given by a Dyson-series,

$$\hat{U}_{\text{eff}}(t) = I + \sum_{k=1}^{\infty}(-i)^k \int_0^t dt_1 \int_0^{t_1} dt_2 \cdots \int_0^{t_{n-1}} dt_n \hat{H}_{\text{eff}}(t_1)\hat{H}_{\text{eff}}(t_2)\cdots\hat{H}_{\text{eff}}(t_n), \tag{A.20}$$

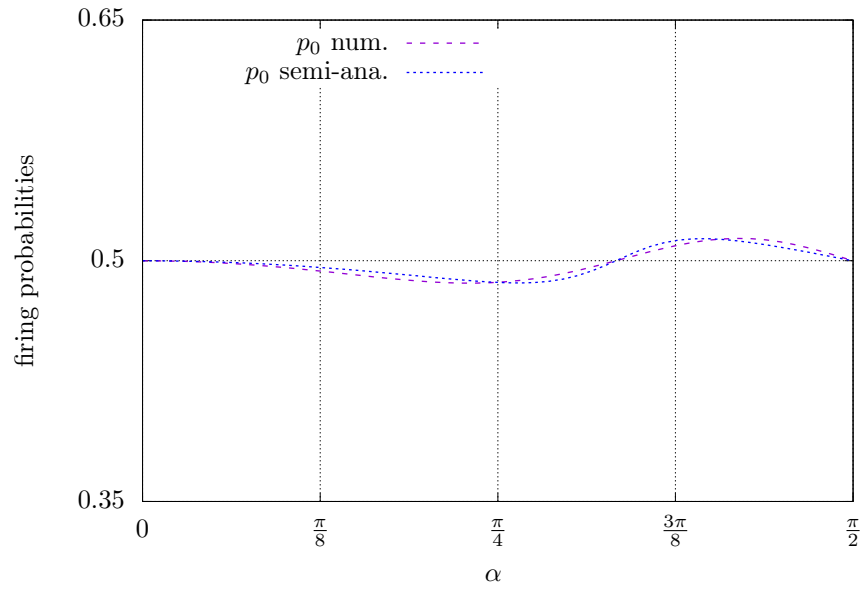

Figure A.2: Firing probabilities of the MZI for $\omega = 0.001$, $\omega_0 = 1$ and $\chi = \frac{\pi}{2}$, $g_g = 0.001$ and $g_d = 0.01$. The dotted line corresponds to the numerical simulation of the MZI whereas the blue line corresponds to the expected value of p_0 if the relative phase equaled the geometric phase.

that yields a formal solution in the limit of $N \to \infty$ under the assumption that the series converges. With this we can obtain approximate solutions by truncating the series.
To sidestep this rather involved procedure we calculated the visibility in the case of the van der Pol spin one system where the spin quantization axis is slowly rotated as follows. First we compute $\hat{U}_{\text{eff}}(t)$ as if the system were not rotated and then subsequently add the known contributions of the geometric phase that we get from the semi-analytical formula:

$$\nu = \left| \text{tr}\left(\hat{U}(t)\hat{\rho}_{0_S} \sum_k e^{\gamma_k(t)} \left|\phi_k(0)\right\rangle \left\langle\phi_k(0)\right| \right) \right|, \tag{A.21}$$

where $\gamma_k(t)$ is the geometric phase of the k-th eigenstate $\phi_k(0)$ of $\hat{\rho}_S(t=0)$.

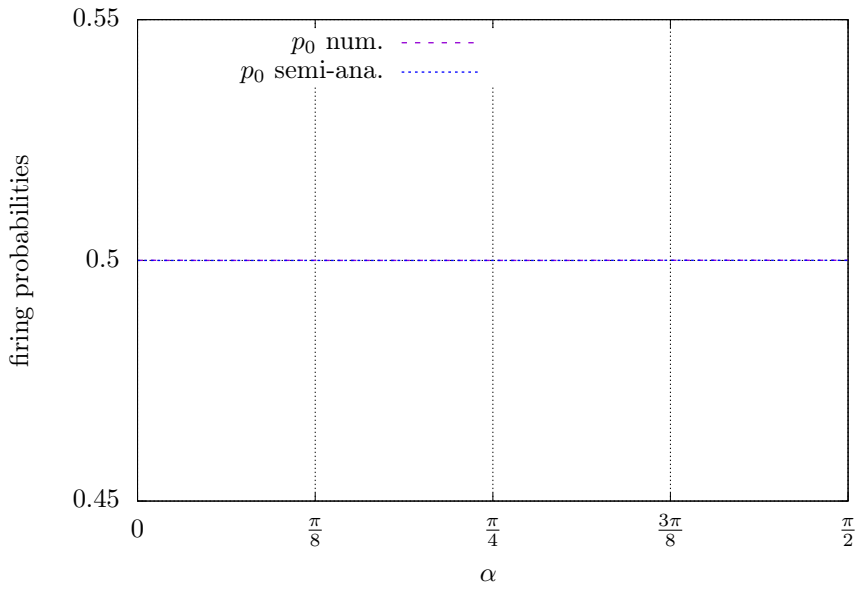

Figure A.3: Firing probabilities of the MZI for $\omega = 0.001$, $\omega_0 = 1$ and $\chi = \frac{\pi}{2}$, $g_g = 0.01$ and $g_d = 0.1$. As can be seen in Fig. A.1, the visibility for this case is so small that no interference pattern can be seen.

Appendix B

The QuantumOptics.jl package

To simulate the Mach-Zehnder interferometer we utilized the QuantumOptics package [8] in the programming language Julia. This package is similar to the Python package QuTip but is built exlusively in Julia. Below a simple example of how we used the functionalities of the package to solve the QMEs governing our system's behaviour.

```
using QuantumOptics

## Parameters
ω0 = 1
gg = 0.01
gd = 0.1

## Basis
b = SpinBasis(1)                        # defining basis of Spin-1 system
Sm = sigmam(b)                          # lowering operator
Sp = sigmap(b)                          # raising operator
Sz = 1/2*sigmaz(b)
Sx = 1/2*sigmax(b)
Sy = 1/2*sigmay(b)

## Model
Γ1 = sqrt(gg/2)*(sqrt(2)*Sz*Sp-Sp*Sz) # Jump operator 1
Γ2 = sqrt(gd/2)*(Sm*Sm)                 # Jump operator 2
function H_sys(t,ρ)                     # System Hamiltonian
    H = ω0*Sz
    J = [Γ1, Γ2]
    Jdagger = dagger.(J)
    return H, J, Jdagger
end

## time evolution
tspan = Array(LinRange(0,2*pi,100))
tout, ρt = time evolution.master_dynamic(tspan, ρ_sys, H_sys;)
```

B.1 Mach-Zehnder-Interferometer

Following is the function used to simulate the Mach-Zehnder-interferometer and produce the firing probabilities p_0, p_1 for a given input state ρ_{sys}, system Hamiltonian H_{sys}, phase shift χ and simulation parameters.

```
function mach_zehnder_interferometer_time_resolved(
        ρsys,H_sys,χ,p_master_dynamic
    )
    # get the system's basis from its density operator
    bsys = basis(ρsys)

    # define identity operator of the system
    Isys = identityoperator(bsys)

    # select the input port of the MZI
    beam0 = 1
    beam1 = 1 - beam0

    # unwrap parameters of master_dynamic
    maxi, err, tspan = p_master_dynamic

    # define basis of beam system
    f = FockBasis(1)
    f1 = Ket(f, [1,0])
    f2 = Ket(f, [0,1])

    # define final time
    T = tspan[end]

    # define beam-splitter operator
    bs = Isys ⊗ ((  projector(f1)
                  - projector(f2)
                  + (f1 ⊗ dagger(f2))
                  + (f2 ⊗ dagger(f1)))/sqrt(2))

    # define phase-shift operator
    ps = Isys ⊗ ((exp(im * χ) * projector(f1)) + projector(f2))

    # define initial state of the beam
    ρbeam = beam0 * projector(f1) + beam1 * projector(f2)

    # initial state of the MZI
    ρin = ρsys ⊗ ρbeam

    # apply first beam splitter
    ρ1 = bs * ρin * dagger(bs)

    # calculate the time evolution
    tout, ρt = time evolution.master_dynamic(
        tspan, ρ1,
        (t,ρ) -> H_mzi(
            t,ρ,ρsys,H_sys,0,f1,f2,Isys,
        );
        maxiters=maxi, reltol=err, abstol=err
    )

    # apply phase shift and second beam splitter to each state
    ρ2 = map(rho -> (ps * rho * dagger(ps)), ρt)
    ρ3 = map(rho -> (bs * rho * dagger(bs)), ρ2)

    # extract firing probabilities
    p0 = map(rho -> (expect(projector(f1), ptrace(rho,1))), ρ3)
    p1 = map(rho -> (expect(projector(f2), ptrace(rho,1))), ρ3)

    # sanity checks
    if maximum(abs.(imag.(p0))) > 10^(-5) || maximum(abs.(imag.(p1))) > 10^(-5)
        throw(error("firing probabilities are imaginary"))
    end

    # return everything
    return real.(p0), real.(p1), tout, ρ2
end
```

the function H_{mzi} used in the above function is given below.

```
function H_mzi(t,ρ,ρsys,H_sys,a,f1,f2,Isys)
    # get system Hamiltonian and jump operators
```

```
    Hsys, Jsys, Jsysdag = H_sys(t,0*ρsys)

    # embed Hsys into MZI Hilbert space
    H = Hsys ⊗ projector(f2) + Isys ⊗ ((-a)*projector(f1))

    # embed all jump operators
    J = repeat([0*(1+im)*H], length(Jsys))
    for k in 1:length(Jsys)
        J[k] = Jsys[k] ⊗ projector(f2)
    end
    Jdagger = dagger.(J)

    return H, J, Jdagger
end
```

Appendix C

Numerical Procedures

C.1 Differentiation

The numerical differentiation to obtain the time derivative of the eigenvectors is done using a fourth order difference quotient from [9]. For n equidistant steps of stepsize h on the intervall $[t_1, t_n]$ the procedure is given as follows:

$$\begin{aligned}
f_1' &= \frac{-25f_1 + 48f_2 - 36f_3 + 16f_4 - 3f_5}{12h}, \\
f_2' &= \frac{-3f_1 - 10f_2 + 18f_3 - 6f_4 + f_5}{12h}, \\
f_i' &= \frac{f_{i-1} - 8f_{i-1} + 8f_{i+1} - f_{i+2}}{12h} \text{ for } 2 < i < n-2, \\
f_{n-1}' &= \frac{-f_{n-4} + 6f_{n-3} - 18f_{n-2} + 10f_{n-1} + 3f_n}{12h}, \\
f_n' &= \frac{3f_{n-4} - 16f_{n-3} + 36f_{n-2} - 48f_{n-1} + 25f_n}{12h}.
\end{aligned} \tag{C.1}$$

This difference quotient is implemented in the following function:

```
function DQ4(vecs,h)

    # determining the size of the input
    n,m = size(vecs)
    # predefining dvecs
    dvecs = Complex.(zeros(n,m))

    # implementing the fourth order difference quotient
    dvecs[1,:] = (-25*vecs[1,:]+48*vecs[2,:]-36*vecs[3,:]
    +16*vecs[4,:]-3*vecs[5,:])
    dvecs[2,:] = (-3*vecs[1,:]-10*vecs[2,:]+18*vecs[3,:]
    -6*vecs[4,:]+vecs[5,:])
    for i in 3:n-2
        dvecs[i,:] = (vecs[i-2,:]-8*vecs[i-1,:]+8*vecs[i+1,:]-vecs[i+2,:])
    end
    dvecs[end-1,:] = (-vecs[end-4,:]+6*vecs[end-3,:]-18*vecs[end-2,:]
    +10*vecs[end-1,:]+3*vecs[end,:])
    dvecs[end,:] = (3*vecs[end-4,:]-16*vecs[end-3,:]+36*vecs[end-2,:]
    -48*vecs[end-1,:]+25*vecs[end,:])
    dvecs = dvecs./(12*h)
    return dvecs
end
```

C.2 Integration

The integrals of the overlap of the eigenstates with their time-derivative are computed using the extended Simpson rule from [10]. For n equidistant steps of size h on the intervall $[t_1, t_n]$ the quadrature is given as follows:

$$\int_{t_1}^{t_n} f(x)\,dx \approx h\left(\frac{3}{8}f_1 + \frac{7}{6}f_2 + \frac{23}{24}f_2 + f_3 + f_4 + \cdots + f_{n-3} + \frac{23}{24}f_{n-2} + \frac{7}{6}f_{n-1} + \frac{3}{8}f_n\right).$$

This quadrature is implemented in the function given below:

```
function ExtSimpsQuad(f,tsteps)

    # extracting stepsize
    dt = tsteps[2]-tsteps[1]

    # check whether the number steps is even
    if length(tsteps)%2 != 0
        throw(error("n has to be even for the Simpson rule to be used"))
    end

    # computing integral
    int = (3/8*f[1]+7/6*f[2]+23/24*f[3])
    for i in 4:length(tsteps)-3
        int += f[i]
    end
    int = int + (23/24*f[end-2]+7/6*f[end-1]+3/8*f[end])

    return dt*int
end
```

C.3 Diagonalization

The diagonalization of the density matrices $\hat{\rho}_k$ given by the solver for the timestep t_k was implemeted by the following function. We adopted the convention that the first entry of each eigenstate was set to be real.

```
function eigensystem(matlist)

    # determine the size of the matrices
    d,d2 = size(matlist[1].data)
    if d2 != d
        throw(error("matrices must be square matrices"))
    end

    # determine how many matrices we have
    n = length(matlist)

    # initializing arrays
    vallist = Complex.(zeros(n,d))
    vecarray = Complex.(zeros(n,d,d))

    # computing
    for i in 1:n
        store = eigen(Array(matlist[i].data))
        vallist[i,:] = store.values
        for j in 1:d
         vecarray[i,j,:] = exp(-im*angle(store.vectors[1,j]))*store.vectors[:,j]
        end
```

```
    end

    return vallist, vecarray
end
```

C.4 Semi-analytical Formula

The semi-analytical implementation of Eq. (1.41) utilizing the difference quotient from Appendix C.1 and the quadrature from Appendix C.2 as well as the diagonalization procedure in Appendix C.3 is given here.

```
function geometric_phase_formula(ρ_sys,H_sys,p_master_dynamic)

    # extracting base and sizes
    bsys = basis(ρ_sys)
    d, ~ = size(ρ_sys.data)

    # unwrapping parameters for the solver
    maxi, err, tspan = p_master_dynamic
    n = length(tspan)

    # time evolution
    tout, ρt = time evolution.master_dynamic(
        tspan, ρ_sys, H_sys; maxiters=maxi,reltol=err,abstol=err
    )

    # diagonalizing time evolution
    vallist, vecarray = eigensystem(ρt)

    # derivatives
    dvecarray = Complex.(zeros(n,d,d))
    h = tout[2]-tout[1]
    for j in 1:d
        dvecarray[:,j,:] = DQ4(vecarray[:,j,:],h)
    end

    # integrals
    farray = Complex.(zeros(n,d))
    intlist = Complex.(zeros(d))
    for i in 1:n
        for j in 1:d
            farray[i,j] = vecarray[i,j,:]'*dvecarray[i,j,:]
        end
    end
    for j in 1:d
        intlist[j] = ExtSimpsQuad(farray[:,j],tout)
    end
    # plugging everything into the formula (11)
    z = Complex(0)
    zp = Complex(0)
    for i in 1:d
        z += (
         sqrt(real(vallist[1,i]*vallist[end,i]))*vecarray[1,i,:]'
         *vecarray[end,i,:]*exp(-im*imag(intlist[i]))
         )
       zp += (
         sqrt(real(vallist[1,i]*vallist[end,i]))*vecarray[1,i,:]'
         *vecarray[end,i,:]
         )
    end
    γ = angle(z)
    vis = abs(z)
    α = angle(zp)
    vis_tong = abs(zp)

    return γ, vis, α, vis_tong, tout, ρt
end
```

Bibliography

[1] A.Wilczek and F. Shapere. *Geometric Phases in Physics*. WORLD SCIENTIFIC, 1989.

[2] M. V. Berry. Quantal phase factors accompanying adiabatic changes. *Proceedings of the Royal Society of London. A. Mathematical and Physical Sciences*, 392(1802):45–57, 1984.

[3] A. Bohm, A. Mostafazadeh, H. Koizumi, Q. Niu, and J. Zwanziger. *The Geometric Phase in Quantum Systems*. Texts and Monographs in Physics. Springer, Berlin, Heidelberg, 1 edition, 2003.

[4] D. Chruściński and A. Jamiolkowski. *Geometric Phases in Classical and Quantum Mechanics*, volume 36 of *Progress in Mathematical Physics*. Birkhäuser, 2004.

[5] M. Ericsson, A. K. Pati, E. Sjöqvist, J. Bränndlund, and D. K. L. Oi. Mixed state geometric phases, entangled systems, and local unitary transformations. *Phys. Rev. Lett.*, 91:090405, Aug 2003.

[6] L. N. Fricker. Geometric phases in limit-cycle systems. Master's thesis, University of Basel, September 2019.

[7] M. Koppenhöfer and A. Roulet. Optimal synchronization deep in the quantum regime: Resource and fundamental limit. *Phys. Rev. A*, 99:043804, Apr 2019.

[8] S. Krämer, D. Plankensteiner, L. Ostermann, and H. Ritsch. Quantumoptics.jl: A julia framework for simulating open quantum systems. *Computer Physics Communications*, 227:109–116, 2018.

[9] J. Li. General explicit difference formulas for numerical differentiation. *Journal of Computational and Applied Mathematics*, 183(1):29–52, 2005.

[10] W. Press, S. Teukolsky, W. Vetterling, and B. Flannery. *Numerical Recipes: The Art of Scientific Computing*. Cambridge University Press, 3 edition, 2007.

[11] A. T. Rezakhani and P. Zanardi. General setting for a geometric phase of mixed states under an arbitrary nonunitary evolution. *Phys. Rev. A*, 73:012107, Jan 2006.

[12] A. Roulet and C. Bruder. Synchronizing the smallest possible system. *Phys. Rev. Lett.*, 121:053601, Jul 2018.

[13] E. Sjöqvist. A new phase in quantum computation. *Physics*, 1:35, 2008.

[14] E. Sjöqvist. Geometric phases in quantum information. *International Journal of Quantum Chemistry*, 115(19):1311–1326, 2015.

[15] E. Sjöqvist, A. K. Pati, A. Ekert, J. S. Anandan, M. Ericsson, D. K. L. Oi, and V. Vedral. Geometric phases for mixed states in interferometry. *Physical Review Letters*, 85(14):2845–2849, Oct 2000.

[16] S. H. Strogatz. *Nonlinear Dynamics and Chaos: With Applications to Physics, Biology, Chemistry and Engineering.* Westview Press, 2000.

[17] D. M. Tong, E. Sjöqvist, L. C. Kwek, and C. H. Oh. Kinematic approach to the mixed state geometric phase in nonunitary evolution. *Phys. Rev. Lett.*, 93:080405, Aug 2004.

[18] J. von Bergmann and H. von Bergmann. Foucault pendulum through basic geometry. *American Journal of Physics*, 75(10):888–892, 2007.